Monthly Notices
of the
ROYAL ASTRONOMICAL SOCIETY

MNRAS **452,** 2018–2033 (2015) doi:10.1093/mnras/stv1284

On the nature of Hα emitters at $z \sim 2$ from the HiZELS survey: physical properties, Lyα escape fraction and main sequence⋆

I. Oteo,[1,2]† D. Sobral,[3,4,5] R. J. Ivison,[1,2] I. Smail,[6] P. N. Best,[1] J. Cepa[7,8] and A. M. Pérez-García[7,8]

[1]*SUPA, Institute for Astronomy, University of Edinburgh, Royal Observatory, Blackford Hill, Edinburgh EH9 3HJ*
[2]*European Southern Observatory, Karl-Schwarzschild-Str. 2, D-85748 Garching, Germany*
[3]*Instituto de Astrofísica e Ciências do Espaço, Universidade de Lisboa, OAL, Tapada da Ajuda, PT1349-018 Lisboa, Portugal*
[4]*Departamento de Física, Faculdade de Ciências, Universidade de Lisboa, Edifício C8, Campo Grande, PT1749-016 Lisbon, Portugal*
[5]*Leiden Observatory, Leiden University, PO Box 9513, NL-2300 RA Leiden, the Netherlands*
[6]*Institute for Computational Cosmology, Durham University, South Road, Durham DH1 3LE*
[7]*Instituto de Astrofísica de Canarias (IAC), E-38200 La Laguna, Tenerife, Spain*
[8]*Departamento de Astrofísica, Universidad de La Laguna (ULL), E-38205 La Laguna, Tenerife, Spain*

Accepted 2015 June 6. Received 2015 June 4; in original form 2014 July 23

ABSTRACT

We present a detailed multiwavelength study (from rest-frame ultraviolet to far-infrared) of narrow-band selected, star-forming (SF) Hα emitters (HAEs) at $z \sim 2.23$ taken from the High-Redshift(Z) Emission Line Survey (HiZELS). We find that HAEs have similar properties and colours derived from spectral energy distributions as *sBzK* galaxies, and probe a well-defined portion of the SF population at $z \sim 2$. This is not true for Lyα emitters (LAEs), which are strongly biased towards blue, less massive galaxies (missing a significant percentage of the SF population). Combining our Hα observations with matched, existing Lyα data, we determine that the Lyα escape fraction ($f_{\rm esc}$) is low (only ∼4.5 per cent of HAEs show Lyα emission) and decreases with increasing dust attenuation, ultraviolet continuum slope, stellar mass and star formation rate (SFR). This suggests that Lyα preferentially escapes from blue galaxies with low dust attenuation. However, a small population of red and massive LAEs is also present, in agreement with previous works and indicating that dust and Lyα are not mutually exclusive. Using different and completely independent measures of the total SFR, we show that the Hα emission is an excellent tracer of star formation at $z \sim 2$ with deviations typically lower than 0.3 dex for individual galaxies. We find that the slope and zero-point of the HAE main sequence at $z \sim 2$ strongly depend on the dust-correction method used to recover the SFR, although they are consistent with previous works when similar assumptions are made.

Key words: galaxies: evolution – galaxies: high-redshift – galaxies: star formation.

1 INTRODUCTION

A wide variety of multiwavelength surveys indicate that the rate at which galaxies form stars has changed with cosmic time, increasing by about one order of magnitude from $z \sim 0$ to $z \sim 1$–2, when the cosmic star formation had a likely maximum (Lilly et al. 1996; Pérez-González et al. 2005; Hopkins & Beacom 2006; Karim et al. 2011; Sobral et al. 2013). A similar behaviour is found for the specific star formation rate (sSFR) – the ratio between the star formation rate (SFR) and stellar mass – at a given stellar mass (Noeske et al. 2007; Dutton, van den Bosch & Dekel 2010; Magdis et al. 2010; Sobral et al. 2014). However, there is still some debate about the behaviour at $z > 2$–3, because there are several uncertain factors involved in the analysis, such as dust-correction factors or the contribution of emission lines in the determination of stellar mass (Bouwens et al. 2009, 2012; Stark et al. 2013; González et al. 2014).

In agreement with the evolution of the cosmic SFR, the molecular gas content of star-forming (SF) galaxies is also higher at $z \sim 2$ than at lower redshifts, although it is claimed that the star-formation efficiency does not strongly depend on cosmic epoch (Daddi et al. 2010; Tacconi et al. 2010; Magdis et al. 2012a,b). The implication

⋆ *Herschel* is an ESA space observatory with science instruments provided by European-led Principal Investigator consortia and with important participation from NASA.

† E-mail: ivanoteogomez@gmail.com

of this is that the increase of the cosmic SFR density with redshift is most likely driven by an increase in the molecular gas mass fraction of galaxies. A change in morphology is also found, from disc-like shapes in the local Universe to clumpy, irregular or compact morphologies at $z \sim 2$ (Elmegreen et al. 2009; Malhotra et al. 2012; Swinbank et al. 2012a,b). Given these rapid changes in galaxy properties, it is important to ensure uniform selection of galaxy samples at different epochs.

Several selection criteria have been traditionally applied to select SF galaxies at $z \sim 2$: (1) the Lyα narrow-band (NB) technique, which selects Lyα emitters (LAEs) by sampling the redshifted Lyα emission line with a combination of NB and broad-band filters (e.g. Ouchi et al. 2008); (2) the Lyman break technique, which selects Lyman-break galaxies (LBGs) by using colours that sample the redshifted Lyman break and includes a rest-frame ultraviolet (UV) colour to rule out low-redshift interlopers (Steidel et al. 2003); (3) the *BzK* criterion (Daddi et al. 2004), which selects SF *BzK* (*sBzK*) galaxies with a double colour selection criterion involving optical and near-infrared (NIR) bands; (4) the BM/BX criteria, which select galaxies within $1 < z < 3$ with different combinations of optical broad-band filters (Adelberger et al. 2004). Other selection criteria are based on far-infrared/submillimetre (FIR/submm) or radio data (Chapman et al. 2005; Riechers et al. 2013), although these identify only the highest SFR systems. The NB technique has also been applied in the NIR regime with the aim to look for Hα emitters (HAEs) at $z \sim 2$ (Bunker et al. 1995; Moorwood et al. 2000; Kurk et al. 2004; Geach et al. 2008; Hayes, Schaerer & Östlin 2010b; Lee et al. 2012; An et al. 2014; Sobral et al. 2013; Tadaki et al. 2013). In this way, it is possible to also use Hα to select and study SF galaxies all the way from the local Universe up to $z \sim 2$ (with Hα moving from the optical into the *K* band). This is a much simpler, self-consistent and well-understood selection; see Sobral et al. (2013), which is the only work so far where Hα emission has been traced from optical to *K* band in a single data set/analysis.

In order to understand the nature of SF galaxies at the peak of galaxy formation and the bias and incompleteness of each selection criterion, it is necessary to compare the physical properties of the galaxy samples selected by the different techniques. This study is important for all evolutionary conclusions based on a given population of galaxies, such as mass–metallicity relations, gas fractions, morphologies, colours, dynamics, etc. (Stott et al. 2013a,b). Furthermore, it provides a way to interpret galaxy evolution studies based on Lyα and Lyman-break techniques, the ones that can be applied at the highest redshifts.

A comparison of the properties of LAEs, LBGs and *sBzK* galaxies has been already done (Grazian et al. 2007; Ly et al. 2009, 2011; Pentericci et al. 2010; Haberzettl et al. 2012; Oteo et al. 2014). Haberzettl et al. (2012) found that the *BzK* criterion is useful to select galaxies at $z \sim 2$, but the samples are biased towards massive SF galaxies and those with red stellar populations. Grazian et al. (2007) report that the *sBzK* criterion is efficient at finding SF galaxies at $z \sim 2$ but is highly contaminated by passively evolving galaxies at red z–K_s colours. They also found that the Lyman-break criterion misses dusty starburst systems. Oteo et al. (2014) found that most LBGs can be selected as *sBzK* galaxies, but most of these do not meet the Lyman-break criterion because this criterion is biased towards blue and/or UV-bright galaxies. Furthermore, they found that *sBzK* galaxies are similar to SF galaxies solely selected by their photometric redshift, and therefore represent an adequate population to study the bulk of SF galaxies at $z \sim 2$. However, the *sBzK* criterion cannot be used to carry out evolutionary studies, unlike the Lyman-break, Lyα or Hα criteria, because of the use of a given filter set for the galaxy selection. However, extensions to higher redshift have been proposed with other broad-band filters (Guo et al. 2012). Additionally, *sBzK* galaxies do not represent by themselves a purely SFR-selected sample, but have a more complicated selection function.

The main objective of this paper is to study the properties of a sample of HAEs at $z \sim 2.23$ selected from the High Redshift(Z) Emission Line Survey (HiZELS; Geach et al. 2008; Sobral et al. 2009b,a, 2012, 2013, 2014). HiZELS uses a set of NB filters in NIR bands to look for emission-line galaxies up to $z \sim 9$. The study of HAEs will also allow us to analyse the accuracy of the Hα emission as a proxy of SFR and the relation between SFR and stellar mass at $z \sim 2$. Combining the Hα observations with available, matched Lyα data, we also study the Lyα escape fraction and its relation to galaxy properties.

This paper is organized as follows. In Section 2, we present the data sets used, the selection of our sources, and how we analyse them. In Section 3, we study the nature of HAEs and compare them with LAEs, LBGs and *sBzK* galaxies to place HAEs into the context of SF galaxies at the peak of cosmic star formation. In Section 4, we study the population of galaxies with both Lyα and Hα emission, and analyse the Lyα escape fraction at $z \sim 2$. We examine in Section 5 the accuracy of Hα emission as a tracer of star formation at $z \sim 2$. In Section 6, we explore the location of our galaxies in an SFR–mass plane and discuss in detail the uncertainties in the determination of the slope of the main sequence (MS) of star formation at $z \sim 2$. Finally, the main conclusions of the work are summarized in Section 7.

Throughout this paper, all stellar masses and SFRs reported are derived by assuming a Salpeter initial mass function (IMF). We assume a flat universe with $(\Omega_m, \Omega_\Lambda, h_0) = (0.3, 0.7, 0.7)$, and all magnitudes are listed in the AB system (Oke & Gunn 1983).

2 METHODOLOGY

2.1 Data sets

Because of the availability of multiwavelength data and NB Lyα and Hα observations over an overlapping redshift range, we focus on the Cosmic Evolution Survey (COSMOS) field (Scoville et al. 2007). In order to sample the SEDs and to study the stellar populations of the galaxies analysed in this paper (see Section 2.2), we take optical to NIR photometry from Ilbert et al. (2013), mid-IR Infrared Array Camera (IRAC) and Multiband Imaging Photometer for *Spitzer* (MIPS) data from the S-COSMOS (Sanders et al. 2007), and *Herschel* Photodetector Array Camera and Spectrometer (PACS) and SPIRE data from the PACS Evolutionary Probe (PEP) and *Herschel* Multitiered Extragalactic Survey (HerMES) projects, respectively (Lutz et al. 2011; Oliver et al. 2012). High-quality photometric redshifts for the studied galaxies are taken from Ilbert et al. (2013). *GALEX* (Zamojski et al. 2007) and *CHANDRA* (Elvis et al. 2009) data are also used.

2.2 Source selection

The main objective of this work is the analysis of the properties of NB-selected HAEs at $z \sim 2.23$. In some sections of this paper, we use a sample of LAEs, LBGs and *sBzK* galaxies at $z \sim 2$ to help us to understand the properties of HAEs and to place them into the context of the SF population at $z \sim 2$. In this section, we explain how all these galaxies were selected.

The samples of HAEs and LAEs are taken from Sobral et al. (2013) and Nilsson et al. (2009), respectively. LAEs and HAEs were selected via the NB technique, with an NB filter centred at 3963 Å (129 Å width) for LAEs and at 2.121 μm (210 Å width) for HAEs. In addition to the NB criterion, HAE selection requires identification of the detected emission line as Hα at $z \sim 2.23$ rather than other line emitters at different redshifts. This selection includes a *BzK* cut to remove low-redshift interlopers, a Lyman-break-like cut to remove $z \sim 3.3$ [O III] emitters, and inclusion of double and triple line emitters from the combination of all HiZELS NB filters. It should be pointed out that the *sBzK* criterion applied to HAEs does not produce the loss of galaxies with unusual colours, but it is used to increase the completeness of the sample. Also, it might be possible that a small number of HAEs have been missed because of their extremely blue SEDs (similar to those for LBGs; see Section 3). However, this percentage is estimated to be very low due to the use of double and triple line detections, because blue HAEs would have very strong emission lines and low reddening, and thus be detectable in [O II] or [O III] as well as Hα (for more details, see Sobral et al. 2013).

Completeness analysis indicates that LAEs are 90 per cent complete down to a Lyα flux of $f_{\mathrm{Ly}\alpha} \sim 6 \times 10^{-17}$ erg cm^{-2} s^{-1} (Nilsson et al. 2009) and HAEs are 90 per cent complete down to an Hα flux of $f_{\mathrm{H}\alpha} \sim 5.6 \times 10^{-17}$ erg cm^{-2} s^{-1} (Sobral et al. 2013). We recall at this point that the Lyα and Hα NB filters used in Nilsson et al. (2009) and Sobral et al. (2013), respectively, select galaxies over an overlapping redshift range. The Lyα filter is broader than the Hα filter in the redshift space, and therefore selects galaxies over a wider redshift range, with the redshift range of HAEs being fully included within the redshift range of LAEs. The great advantage is that it will be possible to study galaxies with both Lyα and Hα emission, even if Lyα has a velocity offset with respect Hα (see Section 4).

It is important to point out that among the whole sample of 187 LAEs of Nilsson et al. (2009), only 118 have a counterpart in the Ilbert et al. (2013) catalogue, which is the data set that we use for optical-to-NIR SED fits. This represents 63 per cent of the sample. The non-detections are mainly a consequence of the blue nature of these LAEs, which are clearly detected in *U*, *B*, *r* or *i* bands, but are very faint in *z* and redder bands. The non-detection in the NIR is an indication of their low stellar mass, being less massive than HAEs and other SF galaxies detected in the NIR. The significant number of LAEs without NIR counterparts indicates that the Lyα technique tends to select low-mass, blue galaxies. Accurate SED fits cannot be carried out for those faint LAEs due to the lack of NIR information that is essential for age, stellar mass and redshift estimations. Stacking might be an alternative, but it has been reported that stacking in LAEs does not provide reliable estimations of the median properties of the population (Vargas et al. 2014). Therefore, we have decided not to include these LAEs in the analysis. This might bias our results because we only include in the final sample the most massive LAEs selected through the NB technique in Nilsson et al. (2009). We indicate the implications of this in the relevant sections of the paper.

Regarding HAEs, most have a counterpart in the Ilbert et al. (2013) catalogue, with only 8 per cent being undetected. The non-detections are mainly due to the faintness of that small population of HAEs in optical bands. At the same time, this is an indication that the HAE selection is also able to identify very dusty sources that might be missed in optical-based studies. We do not include the previous 8 per cent of faint HAEs in our analysis because their UV continuum cannot be well constrained. They represent a very low percentage of the total sample, and therefore their exclusion is not expected to affect significantly the conclusions presented in this work. However, it should be noted that due to their red colours (e.g. high dust extinction) they might be a significant proportion of dust-extinguished HAEs.

LBGs and *BzK* galaxies are taken from Oteo et al. (2014). LBGs were selected with the classical dropout technique, where the near-ultraviolet (NUV) and *U* bands were used to sample the Lyman break at $z \sim 2$ and a *U*–*V* colour was used to avoid contamination from low-redshift interlopers. Furthermore, non-detection in the *GALEX* far-ultraviolet (FUV) band was imposed. The *BzK* galaxies were selected using the criterion of Daddi et al. (2004), which picks up both SF galaxies (*sBzK* galaxies) and quiescent galaxies (*pBzK* galaxies). Because we are interested in galaxies dominated by star formation, we only consider *sBzK* galaxies for most of the analysis presented in this paper, although *pBzK* galaxies will be used for a comparison in some discussions. While LAEs and HAEs have a narrow redshift distribution as a result of their selection with NB filters, LBGs and *sBzK* have redshifts spanning typically $1.5 < z < 2.5$ (Daddi et al. 2004; Oteo et al. 2014). Therefore, in order to carry out a fairer comparison with LAEs and HAEs at $z \sim 2.23$, we additionally limit the photometric redshift of LBGs and *sBzK* galaxies to $2.0 < z_{\mathrm{phot}} < 2.5$. This redshift range has been selected to account for the uncertainties of photometric redshift determinations at $z \sim 2.25$ (Ilbert et al. 2013). To avoid a possible presence of any low-redshift interlopers in the HAE and LAE samples, we also limit their photometric redshifts to the same range: $2.0 < z_{\mathrm{phot}} < 2.5$. Again, this range is chosen to account for the z_{phot} uncertainties.

We clean all samples of contamination from active galactic nuclei (AGNs) by removing all sources with X-ray *CHANDRA* detections (Elvis et al. 2009). It should be pointed out that the percentage of X-ray detections in our galaxies is low, less than 5 per cent in all four samples studied. Additionally, we use *GALEX* photometry (Zamojski et al. 2007) to clean our samples from low-redshift interlopers. At $z \sim 2$, the Lyman break is redshifted out of the UV regime and therefore our galaxies cannot be detected in *GALEX* bands.

After all these considerations, we end up with a sample of 373 HAEs, 69 LAEs, 3751 LBGs and 13 194 *sBzK* galaxies. We note that out of all the samples, HAEs are the ones drawn from the smallest volume, followed by LAEs, LBGs and *sBzK* galaxies. Thus, the number of galaxies in each sample is largely driven by the different volumes. The number density of HAEs is 4.8×10^{-4} Mpc^{-3} down to $\log(L_{\mathrm{H}\alpha}) > 42.0$ and the number density of LAEs is 1.6×10^{-4} Mpc^{-3} down to $\log(L_{\mathrm{Ly}\alpha}) > 42.3$. The number density of LAEs obtained here is smaller than the value reported in Nilsson et al. (2009), mostly due to our inclusion of the criterion to clean the sample from lower-redshift interlopers and because we only include in the sample galaxies detected in the NIR. Furthermore, the value reported in Nilsson et al. (2009) was calculated over 28 per cent of the area covered by their observations, which in turn represents 2 per cent of the entire area of the COSMOS field. This makes their calculation very uncertain, due to the influence of cosmic variance. The number density of LBGs is 3.1×10^{-4} Mpc^{-3}, and the number density of *sBzK* galaxies is the highest in our samples, 1.1×10^{-3} Mpc^{-3}, due to the high number of sources selected. Note also that LBGs and *sBzK* have different, more uncertain SFR limits.

2.3 Analysis

In the rest-frame UV to NIR regime, we analysed the nature of our selected galaxies via the traditional SED-fitting technique,

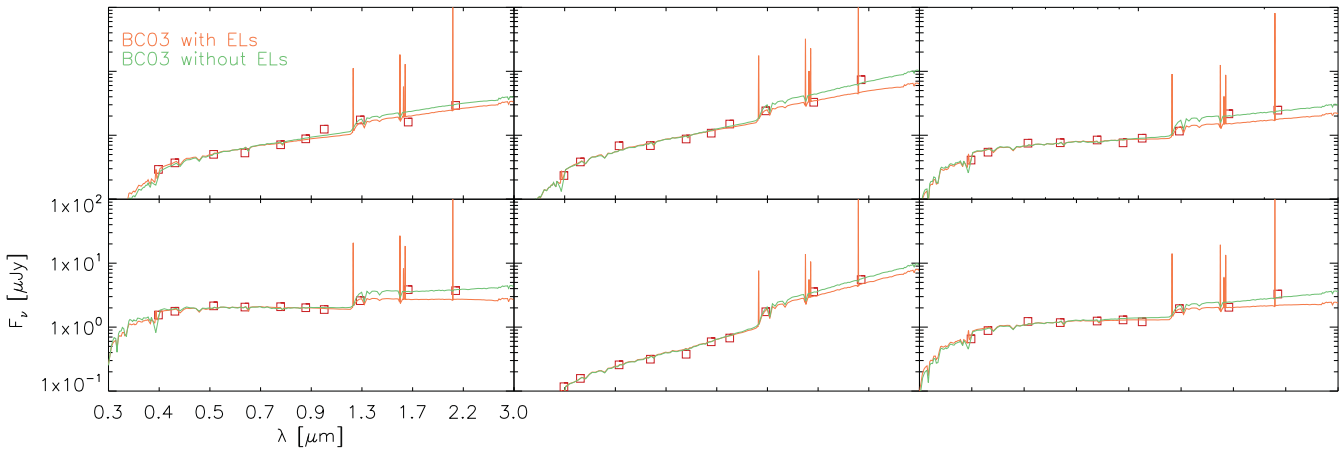

Figure 1. Examples of SED fit results for six randomly selected HAEs from our sample. These fits are representative of the whole sample of HAEs studied in this work. The best-fitting BC03 templates including emission lines are shown in orange, and best-fitting templates with no emission lines are in green. Red open squares are the observed photometric data. Because of the uncertain contribution of the Lyα emission, the U-band information has not been included in the fits. Our HAEs (and also LAEs) are selected for having strong Hα (and Lyα) emission. Therefore, it is expected that emission lines affect their observed fluxes. It can be seen in this figure that the best-fitting templates including emission lines have fainter rest-frame optical continua, and therefore represent less massive galaxies. If templates with no emission lines had been used, the stellar masses would have been overestimated. The UV continuum (and hence SFR_{UV}) of the best-fitting templates does not change significantly when emission lines are included.

using Bruzual & Charlot (2003, hereafter BC03) templates. To this end, we used LEPHARE (Arnouts et al. 1999; Ilbert et al. 2006). We included the emission lines in the stellar population templates (Schaerer & de Barros 2009; de Barros, Schaerer & Stark 2014) because we are working with SF galaxies and, in fact, LAEs and HAEs are selected through their emission lines. The strength of the Lyα emission is more uncertain than other emission lines due to its resonant nature. Therefore, we do not include U-band information in the fits. This does not significantly change the values of the SED-derived properties, because the UV continuum is well sampled with the other filters. In this way, the filters used in the fits are: Subaru B_J, V_J, r^+, i^+, z^+ and VISTA Y, J, H, K_s (Ilbert et al. 2009; McCracken et al. 2012). IRAC data for the IRAC-detected galaxies are also included (Sanders et al. 2007).

The BC03 templates used in this work were built by assuming an exponentially declining SFH and a fixed metallicity $Z = 0.2\,Z_\odot$. We considered time-scale τ_{SFH} values of 0.1, 0.2, 1.0, 2.0, 3.0 and 5.0 Gyr. We chose a fixed value for metallicity because this parameter tends to suffer from large uncertainties (see for example, de Barros et al. 2014). For age, we considered values ranging from 10 Myr to 3.4 Gyr, the age of the Universe at the median redshift of our galaxies. Age values were taken in steps of 10 Myr from 10 to 100 Myr, in steps of 20 Myr from 100 to 200 Myr, in steps of 50 Myr from 200 to 500 Myr, in steps of 100 Myr from 500 Myr to 1 Gyr, and in steps of 0.2 Gyr from 1.0 to 3.4 Gyr. Dust attenuation was included in the templates via the Calzetti et al. (2000) law and parametrized through the colour excess in the stellar continuum, $E_s(B-V)$, for which values ranging from 0 to 0.7 in steps of 0.05 were considered.

Once the templates are fitted, the rest-frame UV luminosity for each galaxy was obtained from its normalized best-fitting template and converted to SFR_{UV} via the Kennicutt (1998) calibration. Note that SFR_{UV} is not corrected for dust attenuation. The UV continuum slope was obtained by fitting a power-law function to the UV continuum of each best-fitting template. Fig. 1 shows the SED fit results for six HAEs randomly selected from our sample. For reference, the best-fitting templates with no inclusion of emission lines (also fitted with LEPHARE) are also included. It can be seen that emission lines have a clear effect on the observed fluxes and the best-fitting rest-frame optical continuum emission. This is because the strongest rest-frame optical emission lines are sampled with some broad-band filters used in the fits: Hα is within the K_s band, [O III]5007 within the H band and [O II]3727 within the J band. While the rest-frame UV SEDs are similar in all the cases, fainter rest-frame optical continua are obtained when including the effect of emission lines. This translates into lower stellar masses and younger ages.

Among the whole sample of SF HAEs, only nine are individually detected in any of the *Herschel* bands. This represents a detection rate of 3 per cent. Interestingly, despite being very low, the percentage of *Herschel* detections is higher for HAEs than for LBGs (∼0.7 per cent) or *sBzK* galaxies (∼0.5 per cent). This indicates that the Hα selection can recover not only relatively dust-free sources, but also highly dust-obscured sources. However, the comparison between the number of *Herschel* detections and physical properties is challenging because at $z \sim 2$ *Herschel* only selects the most extreme galaxies rather than normal SF galaxies. Source confusion is also a major problem when analysing the FIR emission of UV, optical or NIR-selected galaxies. We have attempted to identify source confusion by analysing the optical Advanced Camera for Surveys (ACS) images of the galaxies along with the MIPS 24-μm and Very Large Array (VLA) contours. As an example, see results in Fig. 2 for the three SPIRE 500-μm detected HAEs. The size of the images are 40 arcsec on each side, slightly larger than the SPIRE 500-μm beam, the *Herschel* band with the largest point spread function (PSF). In the three cases, the location of the MIPS detection is coincident with a radio emission, indicating that there is no significant contribution of nearby FIR-bright sources that might contaminate the fluxes in the SPIRE bands. The contamination is even more unlikely in PACS bands, because their PSF is two to four times smaller than SPIRE beams. As a sanity check for SPIRE-detected sources, we have redone the FIR SED fits including only their less-likely contaminated PACS photometry. The values obtained for the total IR luminosity, and hence for SFR_{IR}, are in agreement with those including SPIRE data within the uncertainties (∼0.1–0.2 dex). It should be pointed out that there are two LAEs individually detected in *Herschel* but they are also detected in X-ray and, consequently, have a likely

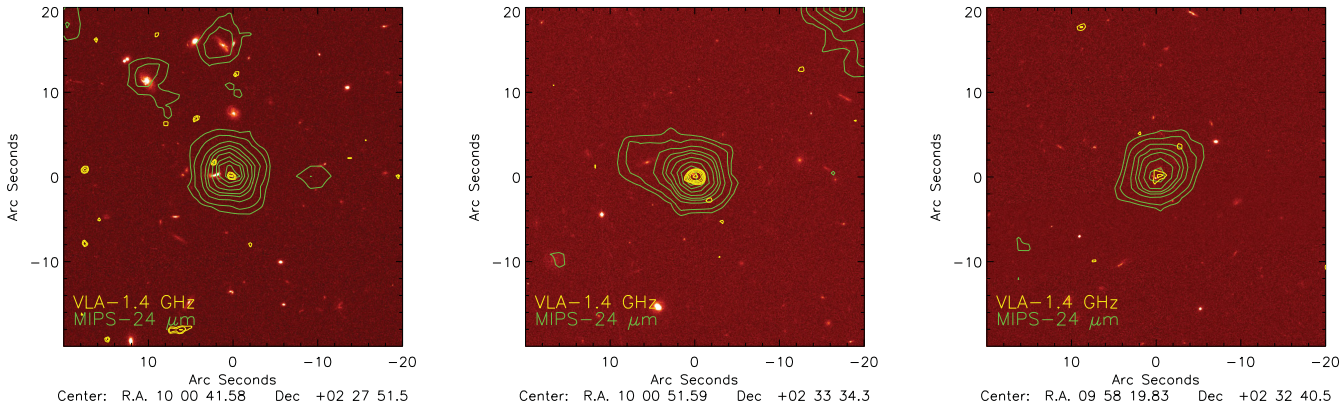

Figure 2. Analysis of source confusion and contamination at FIR wavelengths from nearby sources in the three SPIRE 500-μm detected HAEs. The MIPS 24-μm (green) and VLA (yellow) contours are overplotted in the ACS *I*-band images of the galaxies. HAEs are located in the centre of each image. Images are 40 arcsec on each side, slightly larger than the SPIRE 500-μm beam, the *Herschel* band with the largest PSF. The VLA and MIPS detections, which have better spatial resolution than PACS and SPIRE, indicate that there is no significant contribution of possible nearby FIR-bright sources that might contaminate the HAE *Herschel* fluxes. The PSF of PACS bands is much smaller than the SPIRE PSFs, so contamination is even more unlikely.

AGN nature and are not considered in this work (see Section 2.2 and Bongiovanni et al. 2010).

The IR SEDs of the FIR-detected galaxies are fitted with Chary & Elbaz (2001, hereafter CE01), Dale & Helou (2002), Polletta et al. (2007) and Berta et al. (2013) templates. As an example, we show in Fig. 3 the IR SEDs of the three HAEs detected in SPIRE 500-μm. The presence of the rest-frame 1.6-μm stellar bump (sampled with the IRAC bands at the redshift of our galaxies) is clear in the three galaxies, indicating that their SEDs are dominated by star formation. All the different templates fit well the IR SEDs of the galaxies, with similar values of χ^2_r. We choose to report the results obtained with CE01 templates, as in many previous works in the literature. The best-fitting CE01 templates are integrated between rest-frame 8 and 1000 μm to derive total IR luminosities, $L_{\rm IR}$. These are then converted into SFR by using the Kennicutt 1998 calibration. The total SFR is then obtained by assuming that all the light absorbed by dust in the UV is re-emitted in the FIR: $\rm SFR_{total} = SFR_{UV} + SFR_{IR}$.

Because most galaxies are not individually detected in the FIR, we also performed stacking analysis in *Herschel* bands to study the FIR emission of *Herschel*-undetected galaxies; see, for example, Ibar et al. (2013) for stacking analysis in HAEs at $z \sim 1.47$. One single band near the peak of the dust SED is enough to estimate the total IR luminosity. We focused on the PACS 160-μm band for stacking, due to its relatively small beam, and employ the residual maps, as in many previous works. We stacked by using the publicly available IAS Stacking Library (Béthermin et al. 2010) and uncertainties in the stacked fluxes were derived by using bootstraps. For HAEs, we stacked in different bins of stellar mass [from $\log(M_*/\rm M_\odot) = 9.5$–11 in bins of 0.5 dex] and dust-corrected Hα-derived SFR ($\rm SFR_{H\alpha}$) – from $\log[\rm SFR_{H\alpha}(M_\odot\ yr^{-1})] = 1.0$ to 2.0 in bins of 0.5. Those bins cover the whole range of values for those parameters. For *sBzK* galaxies, where the number of sources is high and allows stacking over more stellar mass bins, we stacked $\log(M_*/\rm M_\odot) = 9.8$–11.6 in bins of 0.2 dex.

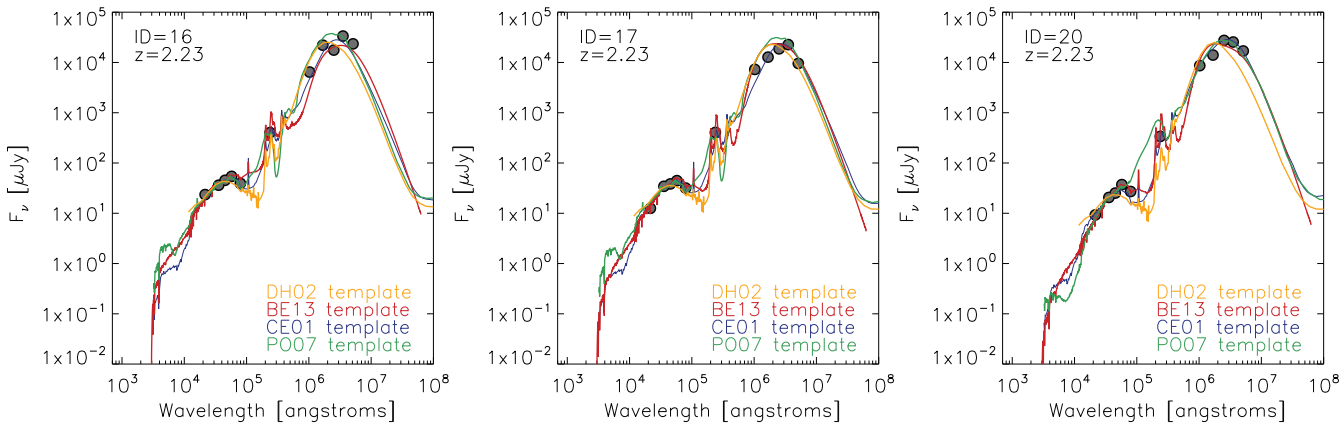

Figure 3. IR SEDs of the three SPIRE 500-μm detected HAEs as an illustration of the SED-fitting results for the *Herschel*-selected galaxies studied in this work. We plot the observed photometry in $K_{\rm s}$, the four IRAC bands, MIPS 24-μm, PACS and SPIRE. The best-fitting Chary & Elbaz (2001), Polletta et al. (2007), Dale & Helou (2002) and Berta et al. (2013) templates are also shown, with the colour code indicated in the bottom-right legend. In the SED fits, a redshift of $z = 2.23$ has been assumed. The data provide a good sampling of the dust emission peak in HAEs at $z \sim 2.23$. Therefore, the integration of the best-fitting templates between 8 and 1000 μm provides an accurate determination of their total IR luminosities and, consequently, dust-corrected SFR. No significant difference is found for $L_{\rm IR}$ when using different templates. We choose to report results obtained with Chary & Elbaz (2001) templates, as in many previous works.

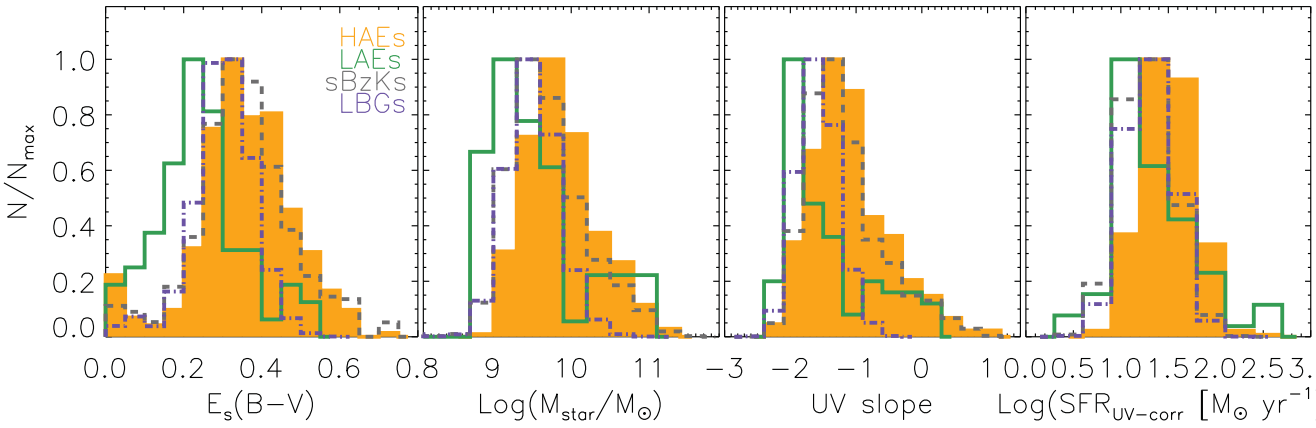

Figure 4. From left to right: dust attenuation, stellar mass, UV continuum slope and dust-corrected total SFR of our selected HAEs (orange-filled histograms). We include the distributions obtained for LAEs, LBGs and *sBzK* galaxies. These properties were obtained by fitting BC03 templates to the observed multiwavelength photometry (from *B* to IRAC bands, when available) of each galaxy. The BC03 templates were built by assuming an exponentially declining SFH and a fixed metallicity of $Z = 0.2\,Z_{\odot}$. Emission lines were also included in the templates. Histograms have been normalized to their maxima in order to clarify the representations. The distributions indicate that HAEs and *sBzK* galaxies have similar stellar populations, both in the median values and in the range covered. HAEs have a very well-defined selection criterion, and therefore represent an excellent sample for studies of star formation at $z \sim 2$. LAEs are significantly biased towards blue, less massive and dust-poor galaxies.

Table 1. Stacked PACS 160-μm fluxes and their associated total IR luminosities for our sample of *sBzK* galaxies at $2.0 < z_{\rm phot} < 2.5$.

Stellar mass range	Stacked $f_{160\,\mu\rm m}$	$\log(L_{\rm IR}/L_{\odot})$
$9.8 \leq \log(M_*/M_{\odot}) < 10.0$	0.53 ± 0.05 mJy	11.4 ± 0.1
$10.0 \leq \log(M_*/M_{\odot}) < 10.2$	0.80 ± 0.06 mJy	11.5 ± 0.1
$10.2 \leq \log(M_*/M_{\odot}) < 10.4$	1.00 ± 0.09 mJy	11.6 ± 0.1
$10.4 \leq \log(M_*/M_{\odot}) < 10.6$	1.20 ± 0.12 mJy	11.7 ± 0.1
$10.6 \leq \log(M_*/M_{\odot}) < 10.8$	1.23 ± 0.12 mJy	11.7 ± 0.1
$10.8 \leq \log(M_*/M_{\odot}) < 11.0$	1.40 ± 0.17 mJy	11.8 ± 0.1

We only detected stacked fluxes for HAEs in the bin corresponding to the highest stellar mass [$10.5 \leq \log(M_*/M_{\odot}) < 11$, where 66 galaxies are included and the stacked flux is $f_{160\mu\rm m} = 1.4 \pm 0.3$ mJy, corresponding to $\log(L_{\rm IR}/L_{\odot}) = 11.8 \pm 0.1$] and highest $\rm SFR_{H\alpha}$ [$1.5 \leq \log(\rm SFR_{H\alpha}) < 2.0$, where 166 sources are included and the stacked flux is $f_{160\mu\rm m} = 1.0 \pm 0.2$ mJy, corresponding to $\log(L_{\rm IR}/L_{\odot}) = 11.3 \pm 0.1$]. This is consistent with more massive SF galaxies being more affected by dust, in agreement with Garn & Best (2010), Sobral et al. (2012) or Ibar et al. (2013), although it could also be due to a pure scaling of the SED. We also stacked LAEs as a function of stellar mass (with the same bins as for HAEs), but no stacked detections are recovered, probably because of the low number of sources producing poor statistics and also the less dusty nature of LAEs (see also Section 3). In *sBzK* galaxies, we recover detections for $9.8 < \log(M_*/M_{\odot}) < 11.0$ with more than 1000 galaxies in each bin. The recovered stacked fluxes are summarized in Table 1. The stacked PACS 160-μm fluxes were converted into $L_{\rm IR}$ by using single-band extrapolations with CE01 templates and errors were obtained from the flux uncertainties. $\rm SFR_{IR}$ were obtained with the Kennicutt (1998) calibration.

3 THE NATURE OF Hα EMITTERS AT $z \sim 2$

Fig. 4 shows the SED-derived dust attenuation, stellar mass, UV continuum slope and dust-corrected SFR of our HAEs at $z \sim 2.23$. It can be seen that HAEs can be either dust-poor (and have blue UV slopes) or dusty (and have red UV slopes) and have a wide range of stellar masses and dust-corrected SFR. This already indicates that our sample of SF HAEs, selected down to a fixed dust-uncorrected SFR, is not significantly biased towards any SED-derived property. The distributions of SED-derived properties of HAEs resemble those for *sBzK* galaxies, one of the classical populations traditionally used to study galaxy properties at $z \sim 2$. However, HAEs seem to have slightly higher stellar masses and SFR on average, probably due to their selection based on SFR. The distributions for HAEs contrast with those found for LAEs, which have much lower dust attenuation and stellar mass, and much bluer UV continuum slopes on average. This indicates that Lyα and Hα samples are formed, on average, by galaxies with different stellar populations (although the values obtained for LAEs are within the distributions found for HAEs). This suggests that the selection based on Lyα is much more biased than the selection in Hα and that using Lyα to select high-redshift galaxies might lead to the loss of a significant population at a given redshift (mostly the reddest and most massive galaxies). Fig. 4 shows that the sample of LBGs is also slightly biased towards galaxies with lower dust attenuation and bluer UV continuum slope, although the effect is not as strong as it is for LAEs.

Fig. 5 shows the relation between colour and stellar mass for our HAEs. We choose the Y–$K_{\rm s}$ colour because it matches at $z \sim 2$ with the rest-frame u–r colour traditionally used to define the blue cloud and the red sequence in the local Universe (see for example, Strateva et al. 2001). Defining a clear difference between the blue cloud and red sequence at $z \sim 2$ is challenging because of the low number of passive galaxies populating the red sequence. However, we consider here that *pBzK* galaxies represent the prototype of passive galaxies populating the red sequence at $z \sim 2$. These galaxies are also represented in Fig. 5. HAEs cover a wide range of colours and stellar masses and thus they represent a diverse population with a range of properties. Hα selection only misses a small population of the bluest and least massive galaxies at $z \sim 2.25$. Some SF HAEs even have colours similar to *pBzK* galaxies, as happens for obscured galaxies with intense, obscured star formation (Oteo et al. 2013b, 2014).

Interestingly, although most galaxies with Lyα emission have low dust attenuation and blue colours, there is a population of 12 red LAEs with $\log(M_*/M_{\odot}) > 10.25$. Their stellar masses are as high as the most massive HAEs. All 12 red LAEs are detected in

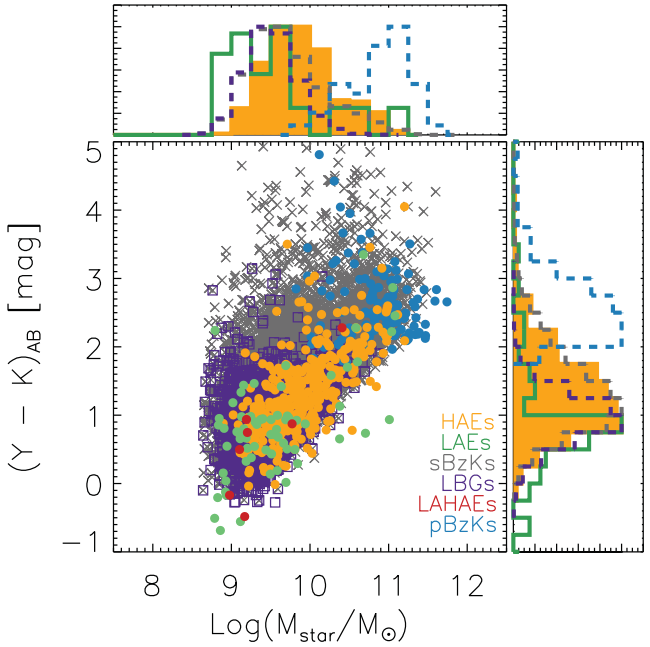

Figure 5. Relation between the *Y*–*K* colour and stellar mass for our sample of HAEs at $z \sim 2.25$. We also represent the location of LAEs, LBGs and *sBzK* galaxies selected in the same field. At the redshift of our galaxies, *Y*–*K* matches the rest-frame *u*–*r* colour used to study the colour distribution and to define the blue cloud and red sequence in local galaxies (Strateva et al. 2001). For reference, we also plot the location of the *pBzK* quiescent population (Daddi et al. 2004) and LAHAEs (see Section 4). We also represent the distributions of *Y*–*K* colour and stellar masses for each type of galaxy but not for LAHAEs, because of their low number. It can be clearly seen that HAEs are well distributed across a wide range of colours and stellar masses as are *sBzK* galaxies. However, LAEs and LBGs are the galaxies with the bluest colours and lowest masses, indicating the biased nature of those selections. LBGs and *sBzK* galaxies are distributed over a larger area because of their wider photometric redshift distributions. Most LAEs are blue and less massive, but there is a small population of LAEs with red colours. Although the number of such red LAEs is not high, it indicates that Lyα emission can also escape from dusty, red systems, as previously reported from individual detections in FIR wavelengths.

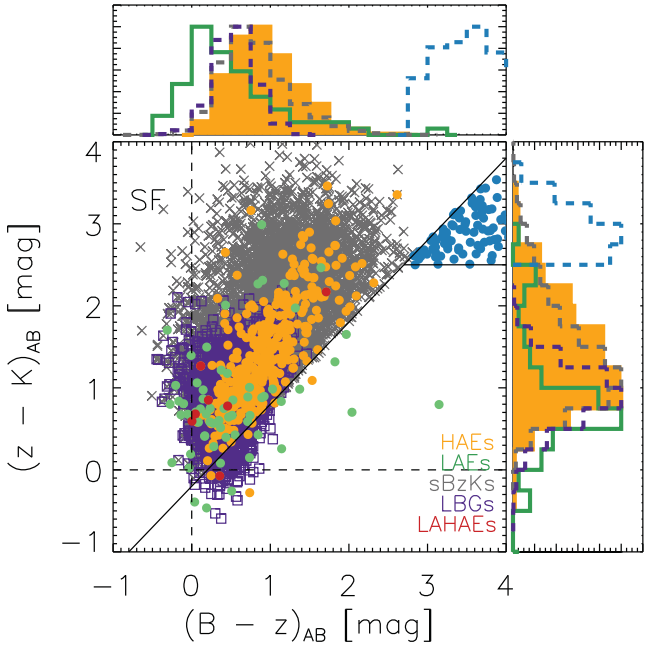

Figure 6. Location of our HAEs at $z \sim 2.25$ in the colour–colour diagram employed to look for *BzK* galaxies at $z \sim 2$ (Daddi et al. 2007). We also represent the location of LAEs, LBGs and LAHAEs (see Section 4). The distributions of *B*–*z* and *z*–*K* colours are also represented for each type of galaxy but not for LAHAEs, because of the low number of galaxies in that sample. It can be seen that most LAEs, LBGs and HAEs can also be selected through the *sBzK* criterion. There is a small population of LBGs (and a less numerous sample of LAEs) that are missed through the *sBzK* criterion, indicating that it misses the bluest and youngest galaxies at $z \sim 2$.

IRAC and there is no indication of power-law-like mid-IR SED, so these red LAEs are SF galaxies rather than AGNs (note that AGN contamination in all our samples has been avoided by discarding galaxies with X-ray detection). This population represents a low fraction of the whole LAE sample, but it indicates that Lyα emission can also escape from dusty, massive and red galaxies, as previously shown via optical colours (Stiavelli et al. 2001) and submm or FIR detections at different redshifts (Chapman et al. 2005; Oteo et al. 2012a,b; Casey et al. 2012; Sandberg et al. 2015). Lyα surveys over larger areas would be needed to increase the samples of red and massive LAEs and to study in detail how and why Lyα can escape from dusty galaxies.

It is also important to examine the overlap between HAEs and other populations of SF galaxies at $z \sim 2.25$. In other words, what is the fraction of galaxies of a given type that could have been selected/missed through any of the other criteria? This study has already been carried out by Oteo et al. (2014) for LBGs, UV-selected and *sBzK* galaxies. They concluded that most LBGs can be also selected through the *sBzK* criterion and only 25 per cent of *sBzK* galaxies would have been selected as LBGs (mainly because of the bias of the Lyman-break selection towards UV-bright galaxies). Consequently, *sBzK* galaxies are a better representation of the bulk of SF galaxies over $1.5 < z < 2.5$ than LBGs.

Fig. 6 represents the classical colour–colour diagram employed to select high-redshift *BzK* galaxies, both SF and passively evolving (Daddi et al. 2004). Studying the location of our selected HAEs in such a diagram gives information about the overlap between those populations. Most HAEs can be also selected as *sBzK* galaxies. As commented in Section 2.2, this was expected for HAEs because a *BzK* selection was applied in Sobral et al. (2013) to the NB-selected HAEs to avoid contamination from low-redshift interlopers. HAEs cover the same range of colours as *sBzK* galaxies, confirming that they are not strongly biased towards either dust-obscured or dust-free objects. However, as suggested by Fig. 5, the Hα selection might miss the bluest galaxies (now in terms of their *z*–*K* colour) at $z \sim 2.25$, as happens to *sBzK* galaxies. Actually, there is a sub-population of blue LBGs with $BzK = (z\text{–}K)_{\rm AB} - (B\text{–}z)_{\rm AB} \leq -0.2$ and $(B\text{–}z)_{\rm AB} < 1$ that cannot be selected as *sBzK* galaxies. This is mainly because of their blue *z*–*K* colour for their *B*–*z* colour. At $2 < z < 2.5$, the *z*–*K* colour samples the Balmer and 4000-Å breaks and therefore is a proxy of the age of the galaxies: younger galaxies should have bluer *z*–*K* colours. This is further confirmed by the shape of their optical SEDs and ages, because 80 per cent of the blue LBGs are younger than 100 Myr (always under the assumption of exponentially declining SFH and 0.2 $Z_\odot$ metallicity and with the caution of the degeneracies between age, SFH, dust attenuation and metallicity) with nearly flat SEDs (when flux densities are expressed per frequency units). Finally, the colours of LAEs indicate that they are more biased towards bluer galaxies, in agreement with the results obtained from SED fits and Fig. 5.

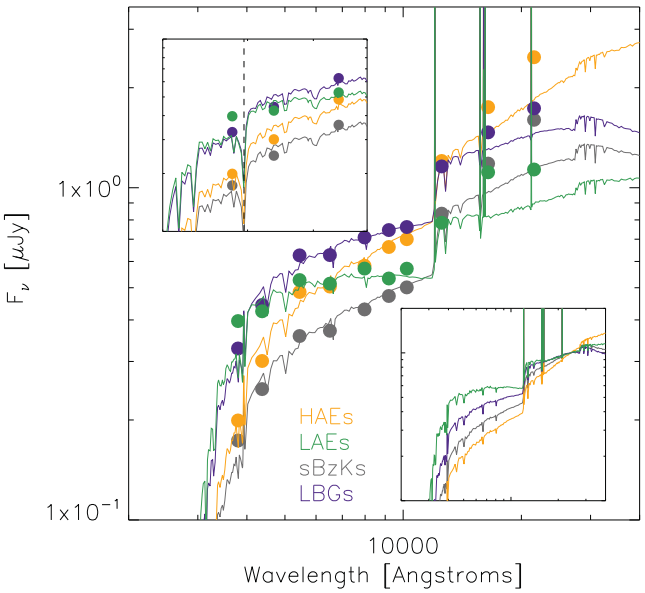

Figure 7. Median SEDs of the HAEs, LAEs, LBGs and *sBzK* galaxies studied in this work. The bottom-right panel shows the median SEDs renormalized to unity at 2.5 μm. In order to explore the equivalent width of the Lyα emission in each sample, we show the region around Lyα in the upper-left panel. In this panel, the location of Lyα emission is indicated with a vertical dashed line. This figure shows that LBGs have a bright rest-frame UV continuum, whereas *sBzK* galaxies are the most attenuated, on average. Except for the difference in the normalization factors, the median SED of HAEs and *sBzK* galaxies are similar, in agreement with the similarity in their stellar populations. The upper-left panel indicates that the Lyα emission boosts the *U*-flux only in LAEs, indicating that LBGs, HAEs and *sBzK* galaxies do not have strong Lyα with high equivalent width, on average.

A significant percentage of HAEs cannot be selected as LBGs because of their faint rest-frame UV continuum. This indicates that a significant population of galaxies with intense Hα emission, and thus actively forming stars, would be missed if only the drop-out criterion had been applied. Along with the relatively high percentage of *sBzK* galaxies that could be missed in the drop-out criterion used in this work, this suggests that the Lyman-break technique employed in this work is biased towards UV-bright galaxies and, consequently, would not be adequate for studying the properties of a complete census of galaxies at the peak of star formation. This result is important for evolutionary studies (Stott et al. 2013a,b; Sobral et al. 2014).

To further analyse the properties of our HAEs, we study their median rest-frame UV-to-optical SED and compare it to the median SED of LAEs, LBGs and *sBzK* galaxies. The median SEDs were built from the median fluxes in each photometric band. Then, following the same procedure presented in Section 2.3, we fitted their observed fluxes with BC03 templates including emission lines. In these fits, we did not include the *U*-band photometry because it might be potentially contaminated by the uncertain strength of the Lyα emission, not included in the templates. The results are shown in Fig. 7. Apart from the normalization factor, the shape of the median SED of HAEs and *sBzK* galaxies is similar, supporting previous results derived with SED-derived properties and observed colours. The SED of HAEs contrast with the median SED of LAEs, which is much bluer, similar to what happens to LBGs. This reinforced previous claims that Lyα selection is strongly biased and might miss a significant percentage of the SF population at the peak of cosmic star formation.

As commented above, the *U* band might be affected by the uncertain strength of the Lyα emission. The top-left inset plot in Fig. 7 shows the region of the SED around the Lyα emission. It can be seen that the *U*-band magnitudes of HAEs, LBGs and *sBzK* galaxies agree well with the best-fitting templates. Therefore, in these galaxies, the equivalent width of the Lyα emission is not high enough to alter significantly the *U*-band fluxes. This indicates that HAEs, LBGs and *sBzK* galaxies do not have Lyα emission with high equivalent width, on average. This is not the case for LAEs. The median *U*-band flux of LAEs is brighter than that predicted by the templates, suggesting intense Lyα emission with high equivalent widths, as expected by their selection. These results indicate that the Lyα emission has high equivalent width only in a small sample of galaxies, reducing the chances of finding strong Lyα emission in a general population of SF galaxies at $z \sim 2$. Our selected LBGs have higher rest-frame UV luminosities than the other galaxies analysed in this work. Their lack of strong Lyα emission, on average, is thus in agreement with the results reported in Schaerer, de Barros & Stark (2011), who found that, at a given redshift, the Lyα emission is more common in galaxies with fainter UV magnitudes (see also Stark et al. 2010).

It should be pointed out that the comparison between the different samples presented in this paper is very dependent on the depth of the surveys used to select them. However, COSMOS is one of the deepest sets of multiwavelength data available. Therefore, it makes a good judgement of the biases that affect samples selected at $z \sim 2$ through the studied selection criteria for most deep extragalactic surveys. One alternative to overcome this limitation would be to use the lensing power of massive clusters of galaxies, as was done by Alavi et al. (2014), allowing us to detect galaxies much fainter than previous surveys at $z \sim 2$. However, this is not the traditional way of selecting LAEs, *sBzK* or HAEs as normally they are searched and analysed in well-known cosmological fields where a wealth of deep multiwavelength observations are available for their analysis.

4 MATCHED LYα AND Hα EMITTERS: LYα ESCAPE FRACTION AT $z \sim 2.23$

Of special interest is the analysis of the galaxies that exhibit both Lyα and Hα emission (Lyα–Hα emitters, LAHAEs), not only because of the low number of such sources reported so far at $z \sim 2$, but also because they allow us to constrain the escape fraction of Lyα photons (Hayes et al. 2010a; Song et al. 2014). As indicated in Section 2.2, we can study LAHAEs because the Lyα and Hα NB filters used in Nilsson et al. (2009) and Sobral et al. (2013) select galaxies within an overlapping redshift slice over the same region of the sky. The Lyα observations select galaxies over the redshift range $2.206 \lesssim z_{\mathrm{Ly}\alpha} \lesssim 2.312$. The Hα observations cover $2.216 \lesssim z_{\mathrm{H}\alpha} \lesssim 2.248$. The Lyα observations cover a wider redshift range than the Hα observations. Therefore, if HAEs had strong Lyα emission, they should have been detected in the Lyα filter.

In the overlapping region of the COSMOS field observed by the Lyα and Hα NB filters, there are 158 HAEs and 146 LAEs.[1] However, there are only seven galaxies in common between the two

[1] We should point out that we include here the whole sample of LAEs, both detected and undetected in NIR wavelengths. The reason is that we are interested in the fraction of HAEs with Lyα emission, not in the SED-derived properties of galaxies with Lyα emission (for which only NIR-detected LAEs should be included; see Section 2.2). The seven LAHAEs have detection in NIR wavelengths, so good SED fits can be carried out.

samples. Therefore, only 4.5 per cent of HAEs have strong enough Lyα emission to be selected as LAEs. This implies very low Lyα escape fraction at $z \sim 2$ and agrees with Hayes et al. (2010a), who found six LAHAEs in their sample, implying an average Lyα escape fraction of $\sim$5 per cent. These results reinforce the different nature of the galaxies selected through the Hα and Lyα NB techniques and highlight the low chance of finding galaxies with Lyα emission, at least at $z \sim 2.23$. It should be remarked that the results of Hayes et al. are based on Lyα observations about 10 times deeper than those used in this work. Similarly, the Hα survey in Hayes et al. (2010a) is about two times deeper than HiZELS. However, we cover in this work an area of the sky that is about 20 times higher than in Hayes et al. (2010a). Therefore, the results complement each other in different regimes of Lyα and Hα brightness and area surveyed. We have explicitly indicated in Fig. 6 the location of LAHAEs. Among the seven joint detections, six have blue B–z colours compatible with almost flat UV continuum, whereas one of them has a red SED. Apart from the red LAHAE with SED-derived $E_s(B-V) \sim 0.5$, the remaining LAHAEs have a median dust attenuation of $E_s(B-V) \sim 0.15$. Their ages range between 1 and 900 Myr.

We derive the Lyα escape fraction in our LAHAEs from the ratio between the intrinsic and observed Lyα luminosities and assuming case B recombination, so the intrinsic Lyα emission can be obtained from the intrinsic (dust-corrected) Hα luminosity. In order to make a fair comparison with previous works, the Hα luminosity is corrected for dust attenuation by using the SED-derived $E_s(B-V)$:

$$f_{\rm esc} = \frac{L_{\rm obs}({\rm Ly}\alpha)}{8.7 \times L_{\rm obs}({\rm H}\alpha) \times 10^{0.4 \times E_s(B-V) \times k(\lambda_{\rm H}\alpha)}}. \quad (1)$$

In equation (1), we have assumed that $E_s(B-V) = E_g(B-V)$, as this has been reported in several previous works to happen at high redshift (see for example, Reddy & Steidel 2004; Erb et al. 2006; Reddy et al. 2010). However, it should be remarked that this has not been proven accurately, and will represent one of the major sources of uncertainties in our derived Lyα escape fraction. This uncertainty affects not only our results but also the results reported in most previous works at similar redshifts, because a relation between $E_s(B-V)$ and $E_g(B-V)$ must be assumed.

In Fig. 8, we represent the Lyα escape fraction as a function of the SED-derived dust attenuation, UV continuum slope, stellar mass and dust-corrected SFR$_{\rm H\alpha}$ for our LAHAEs at $z \sim 2.23$. For comparison, we also represent the nine LAHAEs reported in Song et al. (2014) with both Lyα and Hα emission (UV continuum slopes are not provided for individual galaxies in Song et al. 2014). To be consistent, we take the observed Lyα and Hα fluxes and the SED-derived properties from Song et al. (2014) and then the Lyα escape fraction is calculated with equation (1). However, we note that the selection criteria are not the same in both samples. Here we use the classical NB technique to look for LAEs and HAEs, whereas the LAEs in Song et al. (2014) were found through blind spectroscopy and then followed up with NIR spectroscopic observations. Actually, the Lyα luminosities of the LAHAEs in Song et al. (2014) are higher than for the LAHAEs presented in this work. Despite these differences, the Lyα escape fractions derived in both works agree well.

It can be seen from Fig. 8 that the Lyα escape fraction decreases with increasing dust attenuation, as previously reported at similar and lower redshifts (Hayes et al. 2014; Atek et al. 2014; Song

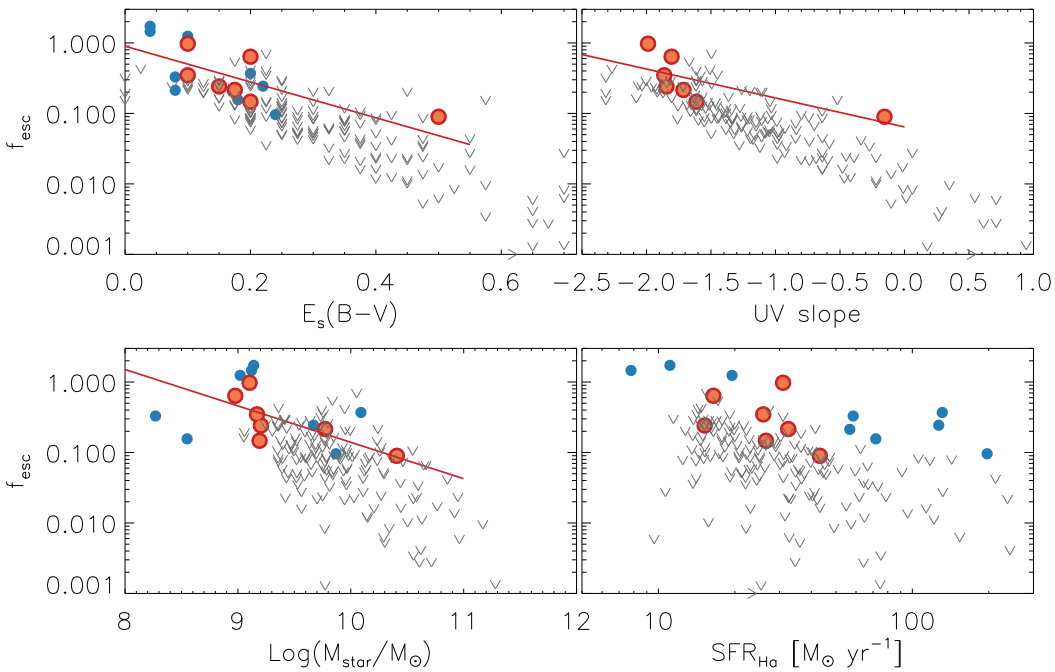

Figure 8. Lyα escape fraction as a function of dust attenuation (upper left), UV continuum slope (upper right), stellar mass (bottom left) and dust-corrected SFR$_{\rm H\alpha}$ (bottom right) for our sample of LAHAEs (orange filled dots). For comparison, we also show the nine galaxies with both Lyα and Hα emission in Song et al. (2014) with blue filled dots (UV continuum slopes are not provided for individual galaxies in Song et al. 2014). The Lyα escape fraction has been calculated by using the SED-derived dust attenuation and assuming that $E_s(B-V) = E_g(B-V)$. This assumption is the main factor affecting the uncertainties of the results, not only in this work, but also in previous results in the literature, because the relation between $E_s(B-V)$ and $E_g(B-V)$ at $z \sim 2$ has not been accurately established yet. The straight lines are linear fits to our points. We also include upper limits for the HAEs undetected in Lyα. It can be seen that the Lyα escape fraction decreases with increasing dust attenuation, redder UV continuum slopes and higher stellar masses and SFRs.

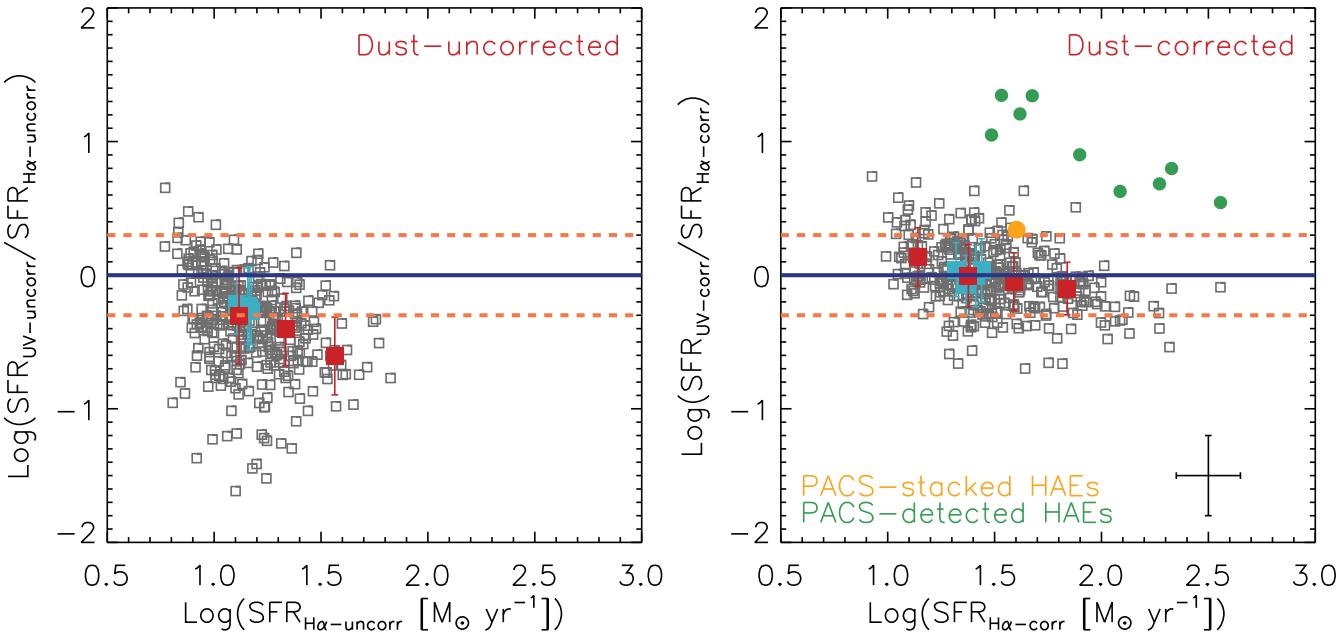

Figure 9. Comparison between the SFR derived from Hα and rest-frame UV luminosities for our studied HAEs at $z \sim 2$. Left panel: results without dust correction. Right panel: results when dust correction is included. The Hα luminosities are corrected by dust attenuation by using the local relation between dust attenuation and stellar mass (Garn & Best 2010), suggested to be valid at least up to $z \sim 1.5$ (Sobral et al. 2012). The rest-frame UV luminosities are corrected by using the dust attenuation derived with the Heinis et al. (2013) relation. In both panels, the filled red squares represent the median SFR_{UV} in different bins of $SFR_{H\alpha}$ and filled cyan squares represent the median SFR_{UV} in different bins of stellar mass. The solid lines are the one-to-one relations and the dashed lines are deviations of ±0.3 dex. PACS-detected and stacked HAEs are represented in the right panel by filled green and orange dots, respectively. The error bars in the right panel show a lower limit on the uncertainties of the results. For the dust correction applied to Hα luminosity, this uncertainty comes from the scatter in the best-fitting relation found in Sobral et al. (2012). It should be pointed out that the uncertainties affecting the dust corrections in Hα are much lower than those affecting the rest-frame UV continuum, as the latter is much more affected by dust.

et al. 2014), and also with increasing (redder) UV continuum slope (a proxy for dust attenuation) and higher stellar mass and SFR. We also include in Fig. 8 the upper limits on the Lyα escape fraction in those HAEs whose Lyα is not detected. These upper limits have been calculated assuming a limiting Lyα EW of 80 Å (Nilsson et al. 2009). The upper limits indicate that the relations found for LAHAEs correspond to the upper envelope of the actual correlations. However, upper limits also indicate that the highest Lyα escape fraction seen at low dust attenuation and/or UV continuum slopes are not seen at higher dust attenuation and/or UV continuum slopes. These results indicate that Lyα emission preferentially escapes from blue, low-mass galaxies with low dust attenuation (with the exception of a low percentage of massive, red and dusty LAEs, as obtained in Section 3). This is in agreement with the SED-derived properties and colours found for LAEs in previous sections. It should be noted that the number of LAHAEs at $z \sim 2$ reported so far is low and, consequently, matched Lyα–Hα surveys over larger areas of the sky are needed to increase the number of LAHAEs and have more robust results with higher statistical significance.

5 Hα SFR VERSUS UV AND UV+IR: A CONSISTENT VIEW

The Hα emission is an excellent tracer of instantaneous star formation and calibrations between the SFR and the Hα luminosity have been proposed in the literature (see for example, Kennicutt 1998). The Hα emission is affected by dust attenuation (although to a much lesser extent than, for example, the UV). Therefore, in order to derive the total SFR from Hα, accurate dust-correction factors are needed. In the local Universe, where a significant percentage of galaxies can be detected in the FIR or their Hα and Hβ emissions can be measured, the dust-correction factors can be determined with acceptable accuracy. However, this is much more challenging for galaxies in the high-redshift Universe, complicating the determination of the total SFR.

In this section, we examine the robustness of the Hα emission as a tracer of SFR at $z \sim 2.23$ for our HAEs. We first compare the results obtained from Hα and UV estimates of the SFR when dust correction is not taken into consideration. This is shown in the left panel of Fig. 9. As can be seen, the two tracers of star formation give significantly different results, with the Hα-derived SFR being higher than that obtained from the rest-frame UV luminosity. The median values found are $SFR_{H\alpha} = 13.7 \pm 9.0\,M_{\odot}\,yr^{-1}$ and $SFR_{UV} = 7.4 \pm 6.6\,M_{\odot}\,yr^{-1}$, where the uncertainties represent the interquartile ranges.

In the right panel of Fig. 9, we show the comparison between Hα-derived and UV-derived SFRs when dust correction is included. We correct the rest-frame UV luminosities by using the relation between the dust attenuation and UV continuum slope derived in Heinis et al. (2013), as in Section 3. The dust correction of the Hα luminosity has been derived by using the relation between stellar mass and dust attenuation of Garn & Best (2010), that has been suggested to be valid for HAEs at least up to $z \sim 1.5$ (Sobral et al. 2012; Ibar et al. 2013; Domínguez et al. 2013; Price et al. 2014). In the right panel of Fig. 9, it can be seen that there is a very good agreement between the UV-derived and the Hα-derived SFRs, despite these being calculated with completely different and independent estimators at

different wavelengths. The difference between the two estimators is typically lower than 0.3 dex for individual galaxies. Furthermore, both estimations agree quite well when galaxies are averaged over different bins of Hα-derived SFR or stellar mass. This result shows the robustness of the Hα emission as a tracer of SFR at $z \sim 2$, which adds to the unbiased and well-understood selection function of the Hα NB method to find SF galaxies at different redshifts (Sobral et al. 2012).

Previous works have also analysed the accuracy of Hα emission to recover SFRs at high redshift (e.g. Erb et al. 2006; Reddy et al. 2010). They correct from dust attenuation derived from SED fitting, $E_s(B-V)$, and assuming $E_s(B-V) = E_g(B-V)$, where $E_g(B-V)$ is the reddening for nebular emission. They actually obtained that the traditionally employed relation $E_s(B-V) = 0.4 \times E_g(B-V)$ (Calzetti et al. 2000) produces Hα SFRs that overpredict those derived from the X-ray and dust-corrected UV emissions. Recently, Steidel et al. (2014) applied a relation between $A_{H\alpha}$ and $E_s(B-V)$ that depends on the value of $E_s(B-V)$. The main advantage of our dust-correction method for Hα emission is that we do not require any assumptions about the relationship between $E_s(B-V)$ and $E_g(B-V)$, which is still until debate and has been suggested to be redshift-dependent (Kashino et al. 2013). Instead, we use a relation between dust attenuation and stellar mass that has been reported to be valid at least up to $z \sim 1.5$ for HAEs (Sobral et al. 2012).

We also compare in the right panel of Fig. 9 the Hα-derived total SFR with the total SFR obtained with direct *Herschel* detections for the nine PACS/SPIRE-detected HAEs. As can be seen, the Hα emission, after the dust correction has been included, is not able to recover the more accurate SFR derived with PACS detections. This is because, at $z \sim 2$, *Herschel* only detects the most extreme sources, for which our average dust-correction factor applied to the Hα luminosity is not high enough (due to very high internal obscuration) to reproduce the more accurate *Herschel*-derived SFR. This also happens to the dust-correction factors derived from the UV continuum slopes in high-redshift *Herschel*-selected galaxies (see for example, Oteo et al. 2013a; Rodighiero et al. 2014). Stacking as a function of the Hα-derived total SFR, we only recover one $>3\sigma$ stacked detection, also represented in the right panel of Fig. 9. The total SFR derived from the PACS stacked flux is higher (by about $\sim$0.3 dex) with respect to the Hα determination. This might indicate that the dust-correction factor used to correct the Hα emission is more uncertain for the most massive HAEs with the highest SFRs, although deeper FIR data would be needed to confirm this trend to more normal SF galaxies with lower SFR.

6 SFR VERSUS STELLAR MASS RELATION AND ITS UNCERTAINTIES AT $z \sim 2$

6.1 Main sequence for HAEs at $z \sim 2$

Most previous works agree that there is a relation between the SFR and stellar mass, commonly referred to as the main sequence (MS), where normal SF galaxies are located (see Speagle et al. 2014 for a recent compilation). The MS has been reported to exist from the local Universe up to high redshift and to be relatively independent of environment (Koyama et al. 2013). However, less is known about the values of its zero-point and slope at a given redshift. One of the main reasons is the lack of FIR detections for a representative population of SF galaxies at each redshift, which prevents accurate determinations of the total SFR. Even with the deepest FIR surveys carried out so far (see for example, Elbaz et al. 2011), only a very small fraction of the galaxies are detected in the FIR, mostly at the highest redshifts (Oteo et al. 2013a, 2014). Furthermore, it is claimed that most high-redshift FIR-detected galaxies are not normal SF galaxies, but likely have a starburst nature and are preferentially located above the MS (Rodighiero et al. 2011; Lee et al. 2013; Oteo et al. 2013a, 2014). Therefore, even with *Herschel*-selected galaxies, it is not possible to determine the slope and zero-point of the MS at high redshift.

Now that we have evidence from Section 5 that the Hα emission is a good tracer of star formation at $z \sim 2.23$, that Hα provides a clean, well-understood, SFR-selected sample (not biased to either just blue or just red galaxies), that HAEs are an excellent representation of the whole population of SF galaxies at $z \sim 2$ (Section 3), and that their stellar masses cover a wider range than many previous studies at $z \sim 2$, we can attempt to study the relation between SFR and stellar mass and its uncertainties by using our sample of HAEs. This is shown by the orange points in Fig. 10, with the best-fitting MS indicated by the red line.

The main caveat of the analysis of the MS with our sample of HAEs is that they are selected down to a fixed $SFR_{H\alpha\ -\ uncorr}$

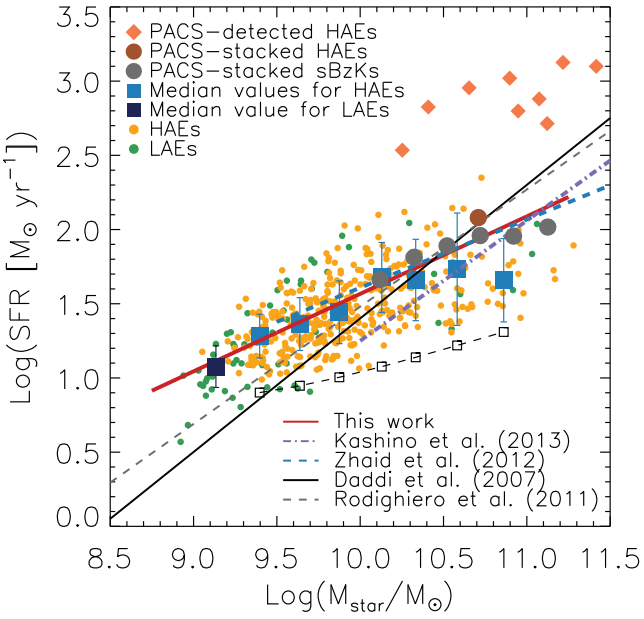

Figure 10. Relation between the SFR and stellar mass for our HAEs at $z \sim 2.23$ (orange dots). Light blue squares represent the median SFR in different bins of stellar mass. The SFR of HAEs is derived with the Kennicutt (1998) calibration and the Hα luminosity corrected from dust attenuation with the local dust–mass relation. The location of *Herschel*-detected and stacked HAEs is indicated with the orange diamonds and brown filled dot, respectively, and their total SFRs are $SFR_{total} = SFR_{UV} + SFR_{IR}$. For comparison, we also show a sample of stacked *sBzK* galaxies with filled grey dots. LAEs are represented with green dots and their SFRs are derived from the dust-corrected rest-frame UV luminosity with the Heinis et al. (2013) relation. Previously reported MS at $z \sim 2$ are overplotted, as indicated in the bottom-right legend. For all the galaxies, the stellar masses have been calculated from SED fitting with BC03 templates including emission lines. The open black squares and dashed curve represent the limiting dust-corrected SFR as a function of mass for our Hα survey (see text for more details). It can be seen from this figure that the HAEs follow an MS with a lower slope than the MS at $z \sim 2$ reported in previous works. Furthermore, our results indicate that there is a flattening of the MS at the highest stellar masses, as previously reported in works from different analysis based on different samples of SF galaxies.

($\sim 3\,M_\odot\,yr^{-1}$ and equivalent width cut; Sobral et al. 2013). Furthermore, the $SFR_{H\alpha\,-\,corr}$ of HAEs is obtained by using a dust-correction factor that depends on the relation between dust attenuation and stellar mass. All of this means that, for a given stellar mass, only HAEs with $SFR_{H\alpha\,-\,corr}$ above a certain limit (i.e. dependent on stellar mass) are included in the sample. This might produce a flattening of the MS with respect to previous works based on other selection functions. In order to explore this in more detail, we have obtained the limiting $SFR_{H\alpha\,-\,corr}$ in different bins of stellar mass. This is represented in Fig. 10 with the open black squares and the dashed curve. As expected, the limiting curve tracks along the locus of the bottom of the points corresponding to HAEs. As an example, our Hα selection would not be able to detect galaxies on the MS relation of Daddi et al. (2007, solid black line on Fig. 10) that have stellar masses $\log(M_*/M_\odot) \sim 9.5$ (but note that dust-correction factors used to recover total SFR are different in Daddi et al. 2007 and this work). If our Hα observations had selected galaxies down to a lower $SFR_{H\alpha\,-\,uncorr}$, we would have been able to select galaxies with lower $SFR_{H\alpha\,-\,corr}$ at that stellar mass and, consequently, we might have obtained a steeper MS. This reflects the effect of our Hα selection on the slope of the MS at $z \sim 2$ and should be taken into account in any comparison with the results presented in the literature for galaxies selected in a different way. However, as shown in Section 6.2, when we use the same methods as in other works to determine the $SFR_{H\alpha\,-\,corr}$ and stellar mass, the MSs are in very good agreement.

It is clear from Fig. 10 that an MS for HAEs exists at $\log(M_*/M_\odot) > 9.25$: more massive HAEs have higher SFRs on average. However, the scatter is significant and it increases with stellar mass. It can also be seen that the MS is flatter for more massive galaxies. Actually, the relation becomes almost flat at $\log(M_*/M_\odot) \geq 10.2$, where the width of the MS is also higher. Because HAEs are selected by star formation, they are truly SF galaxies: all HAEs with $\log(M_*/M_\odot) \geq 10.0$ would also have been selected as SF galaxies according to the *sBzK* criterion. Therefore, the flattening is not caused by the presence of massive quiescent galaxies without star formation. This flattening of the MS towards massive galaxies can also be seen in Heinis et al. (2014) at $z \sim 1.5$ in their work about stacking analysis in *Herschel* bands, although the flattening found in this work is much more significant (see also Oteo 2014, Whitaker et al. 2014, or Schreiber et al. 2015). By fitting a linear relation for galaxies with $\log(M_*/M_\odot) \leq 10.25$ in the form $\log(SFR_{H\alpha-corr}) = a + b \times \log(M_*/M_\odot)$, we find $a = -3.65 \pm 0.15$ and $b = 0.52 \pm 0.02$. This MS is in very good agreement with the results shown in Zahid et al. (2012) in a sample of spectroscopically confirmed HAEs over a similar stellar mass range as our sample. This is the most comparable sample to ours that can be found in the literature in terms of both Hα emission and stellar mass range. Kashino et al. (2013) obtained a higher MS slope with a spectroscopically confirmed sample of galaxies with Hα emission, but their galaxies are at a slightly lower median redshift than HAEs in this work and their sample is restricted to more massive galaxies, mainly with $\log(M_*/M_\odot) > 10$. Our MS has a lower slope than the classical MS found in Daddi et al. (2007), probably produced by our selection effect, although different dust-correction factors and methods for stellar mass determination might play a significant role. This will be discussed in more detail in Section 6.2.

PACS-detected HAEs are all well above the HAE MS, as happens for PACS-detected LBGs and *sBzK* galaxies (Oteo et al. 2014; Rodighiero et al. 2014). This indicates that they have an SB nature and do not belong to the population of normal SF galaxies at $z \sim 2$. Actually, our PACS-detected *sBzK* galaxies have even higher SFRs than those in Oteo et al. (2014) due to the shallower PACS data in COSMOS (Lutz et al. 2011). When stacking as a function of stellar mass, we only recover one detection for HAEs, also represented in Fig. 10. The stacked point is in agreement with the Daddi et al. (2007) MS and it is located slightly above the MS for HAEs found in this work. This is compatible with the previous result that the SFR derived from stacking is slightly higher than that derived from Hα in the most massive HAEs. For comparison, we also show the stacked points corresponding to the sample of *sBzK* galaxies. Only the most massive *sBzK* galaxies are detected through stacking. The stacked points for *sBzK* galaxies agree very well with the extrapolation of the MS for $\log(M_*/M_\odot) \leq 10.25$ HAEs towards higher stellar masses. However, the most massive stacked *sBzK* galaxies have higher SFRs than the most massive HAEs. This difference might be because the dust-correction factor employed to recover the total SFR might not be accurate for the most massive galaxies. However, it could also be as a consequence of a different nature between HAEs and *sBzK* galaxies for the most massive objects. The latter would be supported by the shape of their UV-to-NIR SEDs (see Fig. 7), because massive HAEs are bluer than massive *sBzK* galaxies.

As already obtained in Section 3, galaxies selected through the Lyα technique tend to be less massive than HAEs. Furthermore, the Lyα selection allows us to probe down to lower dust-corrected SFRs. This can be used to extend the MS obtained for HAEs down to $\log(M_*/M_\odot) \sim 9$. This is represented by the blue filled squares in Fig. 10. As in Section 3, the dust-corrected SFR for LAEs has been obtained by assuming the infrared excess (IRX)–β relation of Heinis et al. (2013). Interestingly, and despite the effect of our Hα selection on the MS slope, the point for LAEs agrees very well with the extrapolation of the HAE MS to lower stellar masses.

6.2 Uncertainties in the SFR–mass relation

In order to study the uncertainties involving the determination of the slope and zero-point of the HAE MS at $z \sim 2$ and to try to explain in more detail the differences found with previous works, we compare the SFR–mass relation when considering different methods used in the literature to obtain stellar mass and total SFR. We focus first on the dependence of the HAE MS upon the method used for determining stellar mass. This is shown in Fig. 11, where all the SFRs have been derived by correcting the rest-frame UV luminosity with the IRX–β relation of Meurer et al. (1999) for the sake of homogeneity with previous works that are referred to in this section. Therefore, the main difference would be only the determination of stellar mass. We include in Fig. 11 the MS when the stellar mass of HAEs is obtained through our method of SED fits with BC03 templates associated with exponentially declining SFHs and the inclusion of emission lines (blue open squares; see Section 2.3) and also (orange dots) those obtained using the calibration between *BzK* photometry and stellar mass reported in Daddi et al. (2004) (see also Rodighiero et al. 2014). It can be clearly seen that the slope of the HAE MS depends upon the method used for deriving stellar mass, with the slope being lower when stellar masses are derived using SED fits with the inclusion of emission lines. The top-left inset plot of Fig. 11 compares the stellar masses derived with BC03 templates, including the effect of emission lines, with those derived using the Daddi et al. 2004 calibration. It can be seen that they are correlated but do not follow the one-to-one relation, explaining the difference in the MS.

When using the same dust-correction factors and method for stellar mass determination as in Daddi et al. (2007), we find a MS

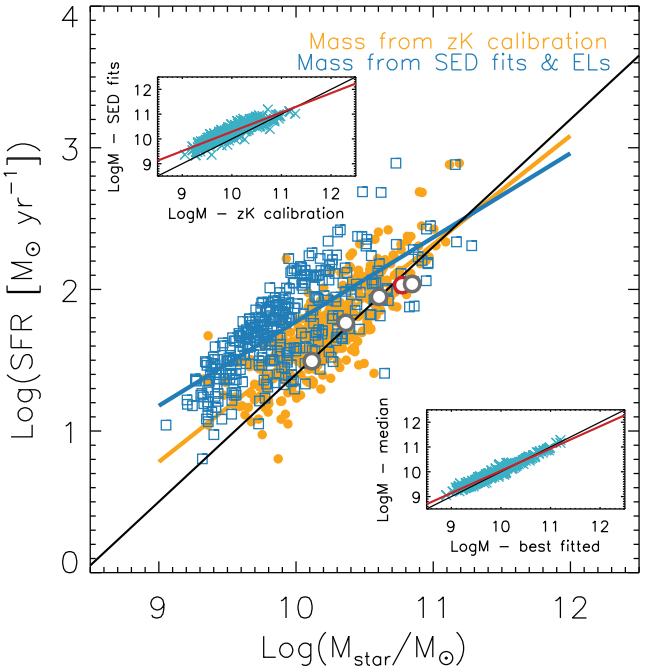

Figure 11. Relation between dust-corrected total SFR and stellar mass for our HAEs when different methods to derive stellar mass are used: SED fits with BC03 templates and inclusion of emission lines (blue open squares) and Daddi et al. (2004) calibration between stellar mass and rest-frame optical colour (orange filled dots). In all cases, we derive dust-corrected total SFR from the rest-frame UV luminosity corrected with the relation of Meurer, Heckman & Calzetti (1999) IRX–β. For comparison, we also show the points associated with stacked *sBzK* galaxies (grey open dots) and HAEs (red open dot) in PACS 160 μm, whose stellar masses are obtained from the Daddi et al. (2004) calibration. Inset panels show the relation between stellar masses when different approaches are considered for their calculation: SED-derived mass against masses obtained with the Daddi et al. (2004) calibration (top-left panel) and SED-derived median versus best-fitting masses (bottom-right panel). In both inset panels, the black line is the one-to-one relation, and the red line is the linear fit to the points. This figure indicates that the definition of the MS (slope and normalization) depends on the way stellar mass is calculated.

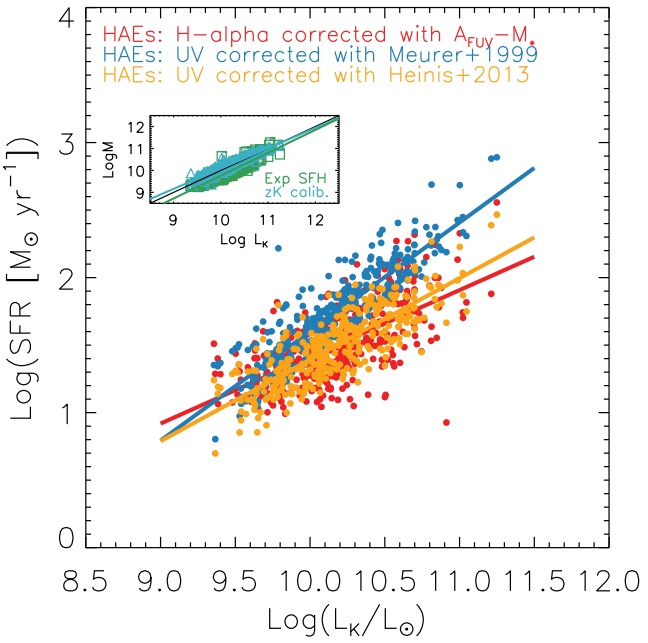

Figure 12. Relation between total SFR and the rest-frame *K*-band luminosity for our sample of HAEs at $z \sim 2.23$. Different estimators of the total SFR have been used: dust-corrected Hα luminosity with the local dust–mass relation (red dots) and dust-corrected UV rest-frame luminosity with the Heinis et al. (2013) (blue) and Meurer et al. (1999) IRX–β (orange) relations. The inset panel shows the relation between the stellar mass and the rest-frame *K*-band luminosity for two different methods for stellar mass: SED fits with BC03 templates (green) and calibration with z and *K* magnitudes (Daddi et al. 2004) (blue). The black line would correspond to mass-to-light ratio equal to unity. Green and blue straight lines are fitted to the green and blue points, respectively. This figure indicates that dust-correction factors have a strong influence on the definition of the MS at $z \sim 2$, both in the slope and zero-point.

slope closer to their result (cf. orange and black lines in Fig. 11). The still slightly lower MS slope might be explained by the Hα selection effect (see Section 6.1). We also plot in Fig. 11 the stacked points for HAEs and *sBzK* galaxies when stellar masses are obtained as in Daddi et al. (2004). It can be seen that they all follow quite well the Daddi et al. (2007) MS, indicating that if stellar masses are calculated in the same manner, then the Daddi et al. (2007) MS is recovered from different SFR estimators (see also Rodighiero et al. 2014). We have also compared the best-fitting stellar masses with the median values as derived by LEPHARE (bottom-right panel in Fig. 11). However, no significant differences are seen between both results that might significantly alter the slope of the HAE MS at $z \sim 2$.

Fig. 12 shows the impact of different dust-correction factors in the definition of the HAE MS at $z \sim 2$. With the aim of avoiding any uncertainty coming from the determination of stellar mass, we represent the SFR–mass relation by using the rest-frame *K*-band luminosity. This luminosity is a proxy of stellar mass (Drory et al. 2004) and is a direct observable quantity that does not need any assumption or calibration in its determination. Three different methods for deriving the total SFR have been employed: dust-corrected Hα luminosity with the local dust–mass relation (red points); dust-corrected rest-frame UV luminosity with the IRX–β relation of Heinis et al. (2013) (orange filled dots); dust-corrected rest-frame UV luminosity with the IRX–β relation of Meurer et al. (1999) (blue filled dots). Note that the only differences in Fig. 12 are the methods adopted for deriving the total SFR. It can be seen that the MS is strongly affected by the different dust corrections, with the slope being steeper with the dust correction based on the Meurer et al. (1999) relation. The MSs derived from the Hα emission assuming the local dust–mass relation and from the rest-frame UV with the dust correction based on the relation of Heinis et al. (2013) are similar because of the agreement between both SFR indicators (see Fig. 9). For reference, we show in the inset panel of Fig. 12 the relation between stellar mass and rest-frame *K*-band luminosity for the two different assumptions for stellar mass determination used in the discussion above.

Summarizing, our results show that, despite evidence that the MS exists, it is a challenge to determine its slope and zero-points at each redshift. Their values depend on the methods employed to obtain stellar mass and total SFR. For given assumptions of these, consistent values can be determined provided that representative samples of sources such as NB-selected HAEs or *sBzK* galaxies are used for their characterization.

7 CONCLUSIONS

In this work, we have carried out a multiwavelength analysis (from the rest-frame UV to the FIR) of the SED of NB-selected, SF HAEs with the aim of analysing their physical properties and their importance for galaxy formation and evolution. We have also compared their physical properties with those derived for other classical populations of SF galaxies at their same redshift: NB-selected LAEs, LBGs and *sBzK* galaxies. The main conclusions of our work are the following.

(i) The HAE selection recovers the full diversity of SF galaxies at $z \sim 2$. Coupled with the simple and well-understood HAE selection (selecting SF galaxies down to a given dust-uncorrected SFR), which can be self-consistently applied at multiple redshift slices from the local Universe up to $z \sim 2.5$, HAEs represent an excellent sample to study galaxy evolution.

(ii) At the depth of the COSMOS data, only about 30 per cent of *sBzK* galaxies can be selected with the drop-out technique, whereas 95 per cent of LBGs can be selected with the *sBzK* criterion. Only 4.5 per cent of HAEs can be selected as LAEs. These results indicate that the Lyman-break and Lyα selections miss a relevant percentage of the SF population at the peak of cosmic star formation. LBGs and LAEs are biased towards blue, less massive galaxies. Although the precise numerical results will depend on the depth of the observations considered in the analysis, these results are important to interpret results at higher redshifts where only Lyα or Lyman-break selections can be applied. However, most LBGs and LAEs can be selected through the *sBzK* criterion. Only the bluest LAEs and LBGs would be missed, although this sample represents a very low percentage of the SF population at $z \sim 2$ and their exclusion would not significantly affect conclusions for galaxy evolution.

(iii) There is a significant percentage of LAEs that are not detected in optical and NIR broad-band filters even with the deep photometry used in this work. The non-detection indicates that these galaxies have a faint continuum but strong emission lines. Because of their non-detection, SED fits cannot be carried out for these galaxies and, consequently, their properties and, most importantly, their contribution to galaxy evolution studies, are unknown.

(iv) Although the Lyα criterion preferentially selects SF galaxies with low dust attenuation and low stellar mass (likely because of the resonant nature of the Lyα emission), there is also a small percentage of red and massive LAEs in our sample, even redder than any LBG in our LBG sample. This indicates that Lyα is also able to escape from dusty and massive galaxies, in agreement with previous work reporting Lyα emission in submm and FIR-selected samples. Because the number of red LAEs is low compared with the total population, surveys over wider areas are needed to study in detail the properties of these galaxies and to shed light on how Lyα can escape from these systems.

(v) The median SEDs of the galaxies studied in this work reveal that the Lyα emission is strong enough to affect the broad-band *U* photometry only in LAEs. This result indicates that Lyα emission is not strong in LBGs, HAEs or *sBzK* galaxies on average, highlighting the low probability of finding Lyα emission in a general sample of selected SF galaxies.

(vi) Only 4.5 per cent of HAEs show detectable Lyα emission, implying low Lyα escape fraction at $z \sim 2$ in agreement with previous results. Additionally, we find that the Lyα escape fraction (f_{esc}) decreases with increasing SED-derived dust attenuation, the UV continuum slope, stellar mass and SFR. This suggests that Lyα preferentially escapes from blue galaxies with low dust attenuation, although a population of red LAEs is also present, indicating that dust and Lyα are not mutually exclusive.

(vii) By using completely different and independent methods to recover the total SFR, we find that the Hα emission is an excellent star formation tracer at $z \sim 2$ with deviations typically lower than 0.3 dex for individual galaxies. These deviations are close to zero when averaging the sample in stellar mass or SFR bins.

(viii) By using the Hα-derived SFR, we study the relation between SFR and stellar mass for our HAEs. We find a MS of star formation, but with a slope lower than the classical Daddi et al. (2007) relation. By fitting a linear function in the form $\log \mathrm{SFR} = a + b \times \log(M/\mathrm{M}_{\odot})$, we obtain $a = -3.65 \pm 0.15$ and $b = 0.52 \pm 0.02$. We show that, in part, the lower slope with respect to previous works might be due to the different selection criteria. However, exploring the uncertainties in the slope and zero-point of the HAE MS, we find that they are very sensitive to both the dust-correction factors adopted to recover the total SFR and the way the stellar masses are determined. This largely explains the difference with previous works and represents the main uncertainty in the definition of MS at high redshift. This might apply to any sample of SF galaxies. Using the same methods for stellar mass calculation and dust correction as in Daddi et al. (2007), we find consistent results for the MS at $z \sim 2$ for our HAEs and also for *sBzK* galaxies whose total SFRs are obtained with a stacking analysis in *Herschel* bands.

ACKNOWLEDGEMENTS

The authors acknowledge the anonymous referee for a detailed and constructive report that has improved the presentation of the results. IO and RJI acknowledge support from the European Research Council (ERC) in the form of Advanced Grant, COSMICISM. DS acknowledges financial support from the Netherlands Organization for Scientific Research (NWO) through a Veni fellowship, from *Fundação para a Ciência e a Tecnologia* (FCT) through a FCT Investigator Starting Grant and Start-up Grant (IF/01154/2012/CP0189/CT0010) and from FCT grant PEst-OE/FIS/UI2751/2014. IRS acknowledges support from STFC (ST/L00075X/1), the ERC Advanced Investigator programme DUSTYGAL 321334 and a Royal Society/Wolfson Merit Award. PNB acknowledges support from STFC. *Herschel* is an ESA space observatory with science instruments provided by European-led Principal Investigator consortia and with important participation from NASA. The *Herschel* spacecraft was designed, built, tested and launched under a contract to ESA managed by the *Herschel/Planck* Project team by an industrial consortium under the overall responsibility of the prime contractor Thales Alenia Space (Cannes), and including Astrium (Friedrichshafen) responsible for the payload module and for system testing at spacecraft level, Thales Alenia Space (Turin) responsible for the service module, and Astrium (Toulouse) responsible for the telescope, with in excess of a hundred subcontractors. PACS has been developed by a consortium of institutes led by MPE (Germany) and including: UVIE (Austria); KUL, CSL, IMEC (Belgium); CEA, OAMP (France); MPIA (Germany); IFSI, OAP/AOT, OAA/CAISMI, LENS, SISSA (Italy); IAC (Spain). This development has been supported by the funding agencies BMVIT (Austria), ESA-PRODEX (Belgium), CEA/CNES (France), DLR (Germany), ASI (Italy) and CICYT/MICINN (Spain). The HerMES data were accessed through the HeDaM data base (http://hedam.oamp.fr) operated by CeSAM and hosted by the Laboratoire d'Astrophysique de Marseille.

REFERENCES

Adelberger K. L., Steidel C. C., Shapley A. E., Hunt M. P., Erb D. K., Reddy N. A., Pettini M., 2004, ApJ, 607, 226
Alavi A. et al., 2014, ApJ, 780, 143
An F. X. et al., 2014, ApJ, 784, 152
Arnouts S., Cristiani S., Moscardini L., Matarrese S., Lucchin F., Fontana A., Giallongo E., 1999, MNRAS, 310, 540
Atek H., Kunth D., Schaerer D., Mas-Hesse J. M., Hayes M., Östlin G., Kneib J.-P., 2014, A&A, 561, A89
Berta S. et al., 2013, A&A, 551, A100
Béthermin M., Dole H., Beelen A., Aussel H., 2010, A&A, 512, A78
Bongiovanni A. et al., 2010, A&A, 519, L4
Bouwens R. J. et al., 2009, ApJ, 705, 936
Bouwens R. J. et al., 2012, ApJ, 754, 83
Bruzual G., Charlot S., 2003, MNRAS, 344, 1000 (BC03)
Bunker A. J., Warren S. J., Hewett P. C., Clements D. L., 1995, MNRAS, 273, 513
Calzetti D., Armus L., Bohlin R. C., Kinney A. L., Koornneef J., Storchi-Bergmann T., 2000, ApJ, 533, 682
Casey C. M. et al., 2012, ApJ, 761, 139
Chapman S. C., Blain A. W., Smail I., Ivison R. J., 2005, ApJ, 622, 772
Chary R., Elbaz D., 2001, ApJ, 556, 562 (CE01)
Daddi E., Cimatti A., Renzini A., Fontana A., Mignoli M., Pozzetti L., Tozzi P., Zamorani G., 2004, ApJ, 617, 746
Daddi E. et al., 2007, ApJ, 670, 156
Daddi E. et al., 2010, ApJ, 713, 686
Dale D. A., Helou G., 2002, ApJ, 576, 159
de Barros S., Schaerer D., Stark D. P., 2014, A&A, 563, A81
Domínguez A. et al., 2013, ApJ, 763, 145
Drory N., Bender R., Feulner G., Hopp U., Maraston C., Snigula J., Hill G. J., 2004, ApJ, 608, 742
Dutton A. A., van den Bosch F. C., Dekel A., 2010, MNRAS, 405, 1690
Elbaz D. et al., 2011, A&A, 533, A119
Elmegreen B. G., Elmegreen D. M., Fernandez M. X., Lemonias J. J., 2009, ApJ, 692, 12
Elvis M. et al., 2009, ApJS, 184, 158
Erb D. K., Steidel C. C., Shapley A. E., Pettini M., Reddy N. A., Adelberger K. L., 2006, ApJ, 647, 128
Garn T., Best P. N., 2010, MNRAS, 409, 421
Geach J. E., Smail I., Best P. N., Kurk J., Casali M., Ivison R. J., Coppin K., 2008, MNRAS, 388, 1473
González V., Bouwens R., Illingworth G., Labbé I., Oesch P., Franx M., Magee D., 2014, ApJ, 781, 34
Grazian A. et al., 2007, A&A, 465, 393
Guo Y. et al., 2012, ApJ, 749, 149
Haberzettl L., Williger G., Lehnert M. D., Nesvadba N., Davies L., 2012, ApJ, 745, 96
Hayes M. et al., 2010a, Nat, 464, 562
Hayes M., Schaerer D., Östlin G., 2010b, A&A, 509, L5
Hayes M. et al., 2014, ApJ, 782, 6
Heinis S. et al., 2013, MNRAS, 429, 1113
Heinis S. et al., 2014, MNRAS, 437, 1268
Hopkins A. M., Beacom J. F., 2006, ApJ, 651, 142
Ibar E. et al., 2013, MNRAS, 434, 3218
Ilbert O. et al., 2006, A&A, 457, 841
Ilbert O. et al., 2009, ApJ, 690, 1236
Ilbert O. et al., 2013, A&A, 556, A55
Karim A. et al., 2011, ApJ, 730, 61
Kashino D. et al., 2013, ApJ, 777, L8
Kennicutt R. C., Jr, 1998, ARA&A, 36, 189
Koyama Y. et al., 2013, MNRAS, 434, 423
Kurk J. D., Pentericci L., Overzier R. A., Röttgering H. J. A., Miley G. K., 2004, A&A, 428, 817
Lee J. C. et al., 2012, PASP, 124, 782
Lee N. et al., 2013, ApJ, 778, 131
Lilly S. J., Le Fevre O., Hammer F., Crampton D., 1996, ApJ, 460, L1
Lutz D. et al., 2011, A&A, 532, A90
Ly C. et al., 2009, ApJ, 697, 1410
Ly C., Malkan M. A., Hayashi M., Motohara K., Kashikawa N., Shimasaku K., Nagao T., Grady C., 2011, ApJ, 735, 91
Magdis G. E., Rigopoulou D., Huang J.-S., Fazio G. G., 2010, MNRAS, 401, 1521
Magdis G. E. et al., 2012a, ApJ, 760, 6
Magdis G. E. et al., 2012b, ApJ, 758, L9
Malhotra S., Rhoads J. E., Finkelstein S. L., Hathi N., Nilsson K., McLinden E., Pirzkal N., 2012, ApJ, 750, L36
McCracken H. J. et al., 2012, A&A, 544, A156
Meurer G. R., Heckman T. M., Calzetti D., 1999, ApJ, 521, 64
Moorwood A. F. M., van der Werf P. P., Cuby J. G., Oliva E., 2000, A&A, 362, 9
Nilsson K. K., Tapken C., Møller P., Freudling W., Fynbo J. P. U., Meisenheimer K., Laursen P., Östlin G., 2009, A&A, 498, 13
Noeske K. G. et al., 2007, ApJ, 660, L43
Oke J. B., Gunn J. E., 1983, ApJ, 266, 713
Oliver S. J. et al., 2012, MNRAS, 424, 1614
Oteo I., 2014, A&A, 572, L4
Oteo I. et al., 2012a, A&A, 541, A65
Oteo I. et al., 2012b, ApJ, 751, 139
Oteo I. et al., 2013a, A&A, 554, L3
Oteo I. et al., 2013b, MNRAS, 435, 158
Oteo I. et al., 2014, MNRAS, 439, 1337
Ouchi M. et al., 2008, ApJS, 176, 301
Pentericci L., Grazian A., Scarlata C., Fontana A., Castellano M., Giallongo E., Vanzella E., 2010, A&A, 514, A64
Pérez-González P. G. et al., 2005, ApJ, 630, 82
Polletta M. et al., 2007, ApJ, 663, 81
Price S. H. et al., 2014, ApJ, 788, 86
Reddy N. A., Steidel C. C., 2004, ApJ, 603, L13
Reddy N. A., Erb D. K., Pettini M., Steidel C. C., Shapley A. E., 2010, ApJ, 712, 1070
Riechers D. A. et al., 2013, Nat, 496, 329
Rodighiero G. et al., 2011, ApJ, 739, L40
Rodighiero G. et al., 2014, MNRAS, 443, 19
Sandberg A., Guaita L., Östlin G., Hayes M., Kiaeerad F., 2015, preprint (arXiv:1501.06017)
Sanders D. B. et al., 2007, ApJS, 172, 86
Schaerer D., de Barros S., 2009, A&A, 502, 423
Schaerer D., de Barros S., Stark D. P., 2011, A&A, 536, A72
Schreiber C. et al., 2015, A&A, 575, A74
Scoville N. et al., 2007, ApJS, 172, 1
Sobral D. et al., 2009a, MNRAS, 398, L68
Sobral D. et al., 2009b, MNRAS, 398, 75
Sobral D., Best P. N., Matsuda Y., Smail I., Geach J. E., Cirasuolo M., 2012, MNRAS, 420, 1926
Sobral D., Smail I., Best P. N., Geach J. E., Matsuda Y., Stott J. P., Cirasuolo M., Kurk J., 2013, MNRAS, 428, 1128
Sobral D., Best P. N., Smail I., Mobasher B., Stott J., Nisbet D., 2014, MNRAS, 437, 3516
Song M. et al., 2014, ApJ, 791, 3
Speagle J. S., Steinhardt C. L., Capak P. L., Silverman J. D., 2014, ApJS, 214, 15
Stark D. P., Ellis R. S., Chiu K., Ouchi M., Bunker A., 2010, MNRAS, 408, 1628
Stark D. P., Schenker M. A., Ellis R., Robertson B., McLure R., Dunlop J., 2013, ApJ, 763, 129
Steidel C. C., Adelberger K. L., Shapley A. E., Pettini M., Dickinson M., Giavalisco M., 2003, ApJ, 592, 728
Stiavelli M., Scarlata C., Panagia N., Treu T., Bertin G., Bertola F., 2001, ApJ, 561, L37
Steidel C. C. et al., 2014, ApJ, 795, 165
Stott J. P. et al., 2013a, MNRAS, 436, 1130
Stott J. P., Sobral D., Smail I., Bower R., Best P. N., Geach J. E., 2013b, MNRAS, 430, 1158
Strateva I. et al., 2001, AJ, 122, 1861

Swinbank A. M., Smail I., Sobral D., Theuns T., Best P. N., Geach J. E., 2012a, ApJ, 760, 130
Swinbank A. M., Sobral D., Smail I., Geach J. E., Best P. N., McCarthy I. G., Crain R. A., Theuns T., 2012b, MNRAS, 426, 935
Tacconi L. J. et al., 2010, Nat, 463, 781
Tadaki K.-i., Kodama T., Tanaka I., Hayashi M., Koyama Y., Shimakawa R., 2013, ApJ, 778, 114
Vargas C. J. et al., 2014, ApJ, 783, 26
Whitaker K. E. et al., 2014, ApJ, 795, 104
Zahid H. J., Dima G. I., Kewley L. J., Erb D. K., Davé R., 2012, ApJ, 757, 54
Zamojski M. A. et al., 2007, ApJS, 172, 468

This paper has been typeset from a TEX/LATEX file prepared by the author.